Received: 19 December 2018 | Revised: 18 July 2019 | Accepted: 18 July 2019

DOI: 10.1111/bph.14802

RESEARCH PAPER

Myricanol modulates skeletal muscle–adipose tissue crosstalk to alleviate high-fat diet-induced obesity and insulin resistance

Shengnan Shen[1] | Qiwen Liao[1] | Tian Zhang[1] | Ruile Pan[2] | Ligen Lin[1]

[1] State Key Laboratory of Quality Research in Chinese Medicine, Institute of Chinese Medical Sciences, University of Macau, Taipa, Macau, China

[2] Institute of Medicinal Plant Development, Peking Union Medical College, Chinese Academy of Medical Sciences, Beijing, China

Correspondence
Ligen Lin, State Key Laboratory of Quality Research in Chinese Medicine, Institute of Chinese Medical Sciences, University of Macau, Avenida da Universidade, Taipa, Macao 999078, China.
Email: ligenl@um.edu.mo

Funding information
Fundo para o Desenvolvimento das Ciências e da Tecnologia, Grant/Award Number: FDCT 0031/2019/A1; Universidade de Macau, Grant/Award Numbers: MYRG2017-00109-ICMS and MYRG2018-00037-ICMS; National Natural Science Foundation of China, Grant/Award Number: 81872754

Background and Purpose: Skeletal muscle is the predominant site for glucose disposal and fatty acid consumption. Emerging evidence indicates that the crosstalk between adipose tissue and skeletal muscle is critical in maintaining insulin sensitivity and lipid homeostasis. The current study was designed to investigate whether myricanol improves insulin sensitivity and alleviates adiposity through modulating skeletal muscle–adipose tissue crosstalk.

Experimental Approach: The therapeutic effect of myricanol was evaluated on palmitic acid (PA)-treated C2C12 myotubes and high-fat diet (HFD)-fed mice. The crosstalk between myotubes and adipocytes was evaluated using Transwell assay. The cellular lipid content was examined by Nile red staining. The mitochondrial content was assessed by MitoTracker Green staining and citrate synthase activity, and the mitochondrial function was examined by Seahorse assay. Expression of mitochondria-related and insulin signalling pathway proteins was analysed by Western blot, and the irisin level was determined by ELISA kit.

Key Results: Myricanol increased mitochondrial quantity and function through activating AMP-activated protein kinase, resulting in reduced lipid accumulation and enhanced insulin-stimulated glucose uptake, in PA-treated C2C12 myotubes. Furthermore, myricanol stimulated irisin production and secretion from myotubes to reduce lipid content in 3T3-L1 adipocytes. In HFD-fed mice, myricanol treatment alleviated adiposity and insulin resistance through enhancing lipid utilization and irisin production in skeletal muscle and inducing browning of inguinal fat.

Conclusions and Implications: Myricanol modulates skeletal muscle–adipose tissue crosstalk, to stimulate browning of adipose tissue and improve insulin sensitivity in skeletal muscle. Myricanol might be a potential candidate for treating insulin resistance and obesity.

Abbreviations: 2-NBDG, 2-(*N*-(7-nitrobenz-2-oxa-1,3-diazol-4-yl) amino)-2-deoxyglucose; ACC, acetyl-CoA carboxylase; AICAR, 5-aminoimidazole-4-carboxamide ribonucleotide; AMPK, AMP-activated protein kinase; BAT, brown adipose tissue; CD36, cluster of differentiation 36; Cidea, cell death-inducing DNA fragmentation factor α-like effector A; CM, conditioned media; COX2, cytochrome *c* oxidase subunit II; COX7a, cytochrome *c* oxidase polypeptide 7a; DEGs, differentially expressed genes; ECAR, extracellular acidification rate; FCCP, carbonyl cyanide-*p* trifluoromethoxyphenylhydrazone; FDR, false discovery rate; FNDC5, fibronectin type III domain-containing protein 5; GEO, gene expression omnibus; GSEA, Gene Set Enrichment Analysis; GSK3β, glycogen synthase kinase 3β; GTTs, glucose tolerance tests; HDL-C, HDL cholesterol; HFD, high-fat diet; HOMA-IR, homeostasis model assessment of insulin resistance; IRS1, insulin receptor substrate 1; ITTs, insulin tolerance tests; KRP, Krebs–Ringer phosphate; LDL-C, LDL cholesterol; METRNL, meteorin-like protein; MTT, 3-(4,5-dimethylthiazol-2-yl)-2,5-diphenyltetrazolium bromide; OCR, oxygen consumption rate; P/S, penicillin–streptomycin; PA, palmitic acid; PGC-1α, PPARγ coactivator-1α; Prdm16, PR domain containing 16; RD, regular chow diet; SIRT1, NAD^+-dependent deacetylase sirtuin-1; STRING, Search Tool for the Retrieval of Interacting Genes; TG, triglyceride; UCP1, uncoupling protein 1; UCP3, uncoupling protein 3; WAT, white adipose tissue.

1 | INTRODUCTION

Around 451 million adults aged over 18 worldwide are estimated to have diabetes, of which 90% are Type 2 diabetes (IDF, 2017). Type 2 diabetes is a complex chronic illness associated with hyperglycaemia, occurring from inadequate production of **insulin** and/or inability of the target tissues, such as skeletal muscle, adipose tissue, and liver (Chaudhury et al., 2017). Skeletal muscle comprises about 40% of the body mass in humans and is the predominant site for **glucose** disposal and fatty acid consumption. Thus, skeletal muscle insulin resistance is considered to be the primary defect of insulin action (DeFronzo & Tripathy, 2009). Therapeutic methods targeting enhancement of insulin action in skeletal muscle are promising for treatment of Type 2 diabetes.

Although the exact mechanism of the initiating and development of insulin resistance in skeletal muscle is not fully elucidated, accumulation of triglycerides (TGs) and lipid intermediates (ceramides, DAG, etc.) in myotubes has been considered to play an important role. Mitochondria are the main organelles where fatty acids are oxidized. Mitochondrial dysfunction impairs fatty acid transfer and β-oxidation, which results in excess lipid accumulation within skeletal muscle, leading to insulin resistance (Kraegen & Cooney, 2008).

The crosstalk between adipose tissue and skeletal muscle has been recognized to play an important role in insulin sensitivity and adiposity. Adipose and skeletal muscle secrete adipokines and myokines, respectively, to maintain metabolic homeostasis coordinately. Irisin is a myokine, processed from the product of *Fndc5* gene (Boström et al., 2012). Irisin is regulated by **PPARγ** coactivator-1α (**PGC-1α**), to mediate the beneficial effects of exercise on metabolism and induce the browning of white adipose tissue (WAT) by increasing uncoupling protein 1 (**UCP1**) expression (Boström et al., 2012). The decreased circulating irisin level and *Fndc5* gene expression in muscle are correlated with increased body mass index, fasting glucose, and total cholesterol (Huh et al., 2012). Additionally, irisin stimulates muscle accretion by inducing myogenesis and inhibiting muscle atrophy (Demirpence et al., 2016; Huh et al., 2014; Moreno-Navarrete et al., 2013; Rodriguez et al., 2015). AMP-activated protein kinase (**AMPK**) plays a central role in the regulation of fuel metabolism in skeletal muscle. Activation of AMPK stimulates fatty acid consumption and glucose uptake thought enhancing insulin signalling transduction (Kahn, Alquier, Carling, & Hardie, 2005). The AMPK–PGC-1α signalling cascade is essential for maintaining basal *FNDC5* expression and irisin production and secretion to induce exercise-based adaptations in muscle metabolism (Huh et al., 2014). However, there were controversial reports about the circulating irisin concentration in relation to obesity and Type 2 diabetes. Irisin level was found to positively correlated with fat mass and hyperlipidaemia (de la Iglesia et al., 2014; Pardo et al., 2014; Stengel et al., 2013). Physical exercise was not associated with irisin level (Kurdiova et al., 2014).

Myricanol, a diarylheptanoid from Chinese bayberry (*Myrica rubra*), was identified as an AMPK activator in our previous study (Shen et al., 2019). In the current study, we aimed to assess the role of myricanol in improving insulin sensitivity in **palmitic acid** (PA)-treated C2C12 myotubes and high-fat diet (HFD)-fed mice and to investigate whether myricanol regulates irisin production and subsequently induces browning of WAT.

What is already known

- Myricanol is an activator of AMP-activated protein kinase.
- Irisin is a myokine that promotes browning of adipose tissue and increases energy expenditure.

What this study adds

- Myricanol improves insulin sensitivity and reduces adiposity through activating AMP-activated protein kinase.
- Myricanol stimulates irisin production and induces browning of adipose tissue.

What is the clinical significance

- Myricanol provides an insightful perspective to be a candidate for treating insulin resistance and obesity

2 | METHODS

2.1 | Cell culture and differentiation

Mouse C2C12 myoblasts (RRID:CVCL_0188) were obtained from American Type Culture Collection (Manassas, VA) and maintained in DMEM (Gibco) with 10% FBS (Gibco) and 1% penicillin–streptomycin (P/S). To initiate differentiation, the cells were grown to 70–80% confluence and incubated with DMEM containing 2% heat-inactivated horse serum and 1% P/S for 4 days. Media were refreshed every day. The fully differentiated myotubes were used for the following experiments.

Murine preadipocyte 3T3-L1 cells (RRID:CVCL_0123) were obtained from American Type Culture Collection. 3T3-L1 preadipocytes were maintained in DMEM with 10% calf serum (Gibco) and 1% P/S. Two days after confluence (Day 0), cells were treated with DMEM containing 10% FBS, 1 μmol·L−1 of **dexamethasone**, 0.5 mmol·L−1 of **isobutylmethylxanthine** (IBMX), and 5 μg·ml−1 of insulin for 2 days. Cells were then maintained in DMEM with 10% FBS and 5 $\mu g \cdot ml^{-1}$ of insulin for 6 days, and medium was changed every other day. The fully differentiated adipocytes (Day 8) were used for the following experiments. 3T3-L1 adipocytes were fixed with 4% formaldehyde for 20 min. The lipid accumulation of 3T3-L1 cells was evaluated by microscopic observation and Oil Red O staining, as described previously (Lin et al., 2012).

2.2 | PA-induced lipid accumulation in C2C12 myotubes

PA was completely dissolved in 75% (v/v) ethanol by heating at 55°C and then diluted in DMEM containing 1% (w/v) fatty acid-free BSA

(Sigma-Aldrich). The solution was mixed for 2 hr with gentle shaking and then sterilized by passing through 0.2-μm filters. The fully differentiated myotubes were treated with 250 μmol·L^{-1} of PA for 24 hr with or without indicated concentrations of myricanol. The control cells were treated with the same volume of ethanol–BSA–DMEM solution.

2.3 | RNA interference

siRNAs targeting *Ampka1* (mouse, sc-45313) and *Fndc5* (mouse, sc-145214) were purchased from Santa Cruz Biotechnology (Santa Cruz, CA, USA). Scrambled non-targeting siRNA (sc-37007, Santa Cruz) was used as a negative control. C2C12 cells were seeded into six-well plates at a concentration of 5 × 10^5 cells per well. After differentiation, C2C12 myotubes were transfected with 80 nmol·L^{-1} of si*Ampka1*, si*Fndc5*, or scrambled siRNA using Lipofectamine 3000 transfection reagent (Thermo) and incubated at 37°C for 6 hr. Subsequently, cells were switched to fresh medium and incubated for an additional 24 hr. The following experiments were executed.

2.4 | Co-culture of C2C12 myotubes and 3T3-L1 adipocytes

Co-culture assays were performed using Transwell inserts with an 8-μm membrane pore size (Millipore). 3T3-L1 cells were seeded onto the inserts at a density of 5 × 10^4 cells per well and induced to full differentiation. C2C12 myotubes were treated with DMSO as a vehicle control, 5-aminoimidazole-4-carboxamide ribonucleotide (AICAR, 20 μmol·L^{-1}, AMPK activator) as a positive control, compound C (CC, 10 μmol·L^{-1}), or different concentrations of myricanol (1.25, 2.5, and 5 μmol·L^{-1}) for 24 hr. Then, myotubes were switched to fresh medium and cultured for an additional 24 hr. Subsequently, the C2C12-conditioned media (CM) were transferred to 24-well plates containing inserts. After incubation for 24 hr, the 3T3-L1 adipocytes were collected for the following studies. TG level in adipocytes was analysed using commercial kits (Nanjing Jiancheng, Nanjing, China), which was further normalized by protein content.

2.5 | Cell viability

Cell viability was determined by 3-(4,5-dimethylthiazol-2-yl)-2,5-diphenyltetrazolium bromide (MTT) assay as described previously (Feng et al., 2017). C2C12 cells were seeded in 96-well plates at a density of 1 × 10-4 cells per well. The fully differentiated myotubes were treated with the indicated concentrations of myricanol for 24 hr, with or without 250 μmol·L^{-1} of PA. Then cell viability was determined by incubation with DMEM containing MTT (1 mg·ml^{-1}) for 4 hr, followed by dissolving the formazan crystals with 100 μL of DMSO. The absorbance at 570 nm was measured by a SpectraMax M5 microplate reader (Molecular Devices, CA, USA). The calculation equation for relative cell viability was as follows: cell viability (%) = (As − A0)·(Ac − A0)$^{-1}$·100%, where As, A0, and Ac were the absorptions of test sample, blank control, and negative control (DMSO), respectively. Cell viability was further determined by the release level of LDH in the cell culture medium using the LDH Cytotoxicity Assay Kit (Beyotime, Shanghai, China), according to the manufacturer's instructions.

2.6 | Nile red staining

To detect intracellular lipid accumulation, Nile red staining was performed on fully differentiated myotubes. Cells were washed twice with PBS and then incubated with PBS containing 1 μg·ml^{-1} of Nile red for 15 min at 37°C. After washed with PBS twice, the fluorescence was monitored at an excitation wavelength of 488 nm and an emission wavelength of 550 nm, using a SpectraMax M5 microplate reader.

2.7 | MitoTracker Green staining and citrate synthase activity assay

C2C12 cells were seeded with 1.0 × 10^4 cells per well in 96-well plates. After full differentiation, myotubes were treated with 250 μmol·L^{-1} of PA, with or without different concentrations of myricanol, for 24 hr. Subsequently, the cells were stained with MitoTracker Green probes (Beyotime) following the manufacturer's instructions. Fluorescent images were captured with an Olympus flourescence microscope (IX73, Olympus, Tokyo, Japan). Citrate synthase activity was determined with a Citrate Synthase Activity Assay Kit (ab239712, Abcam, Cambridge, UK) following the manufacturer's instructions. Citrate synthase activity was further normalized to protein content.

2.8 | Seahorse analysis

Seahorse XF Cell Energy Phenotype Test Kit (103325-100, Agilent Technologies, Santa Clara, CA, USA) was used to measure the oxygen consumption rate (OCR) and extracellular acidification rate (ECAR) on a Seahorse Bioscience XF24-3 Extracellular Flux Analyzer (Agilent Technologies). C2C12 or 3T3-L1 cells were seeded in XF24-well microplates (Agilent Technologies) at 5 × 10^4 cells per well. After fully differentiated, the cells were incubated in XF assay medium and treated as indicated. Then, the cells were incubated in the absence of CO_2 for 1 hr. XF assay medium was low-buffered bicarbonate-free DMEM (pH 7.4) and replicated the glucose and pyruvate/glutamax composition of the respective experimental conditions. After measuring basal OCR and ECAR, 1 μmol·L^{-1} of oligomycin and 1 μmol·L^{-1} of carbonyl cyanide-*p* trifluoromethoxyphenylhydrazone (FCCP) were introduced in real time, to measure the OCR and ECAR under stressed condition. Subsequently, cellular protein content was quantitated with BCA kit (Life Technologies, Grand Island, NY, USA), and OCR and ECAR were normalized accordingly.

2.9 | Determination of ATP content

Cellular ATP content was measured using an ATP content kit following the manufacturer's instruction (Beyotime, Shanghai, China). The luminescence intensity was measured with a luminometer (SpectraMax M5). ATP level was further normalized to protein content. Results were expressed as relative ATP levels to the control.

2.10 | Western blot analysis

The antibody-based procedures used in this study comply with the recommendations made by the *British Journal of Pharmacology* (Alexander et al., 2018). Western blot analysis was performed as described previously (Li et al., 2018). In brief, protein concentration of each sample was quantified using the BCA protein assay kit. The same amount of proteins (30–50 μg) was separated by SDS-PAGE, transferred to PVDF membranes (Bio-Rad, Hercules, CA, USA), blocked with 5% nonfat milk in TBST buffer (100 mmol·L^{-1} of NaCl, 10 mmol·L^{-1} of Tris–HCl, pH 7.5, and 0.1% Tween 20) for 1 hr at room temperature, and incubated with specific primary antibodies (Table S1) overnight at 4°C. After washing with TBST three times, an HRP-conjugated secondary antibody was added and incubated for 2 hr at room temperature. The immunoblotting signals were developed using a SuperSignal West Femto Maximum Sensitivity Substrate kit (Thermo, Rockford, IL, USA). Then, specific protein bands were visualized using the ChemiDoc MP Imaging System and quantitated using Image Lab 5.1 (Bio-Rad).

2.11 | Glucose uptake assay

Myotubes were incubated with different concentrations of myricanol, with or without PA treatment, for 24 hr. Then, cells were washed with Krebs–Ringer phosphate (KRP) buffer (20 mmol·L^{-1} of HEPES, 137 mmol·L^{-1} of NaCl, 4.7 mmol·L^{-1} of KCl, 1.2 mmol·L^{-1} of $MgSO_4$, 1.2 mmol·L^{-1} of KH_2PO_4, 2.5 mmol·L^{-1} of $CaCl_2$, and 2 mmol·L^{-1} of pyruvate; pH 7.4) and incubated in KRP buffer with 0.2% BSA for 3 hr. To stimulate glucose uptake, cells were incubated with KRP buffer containing 0.1 μmol·L^{-1} of insulin for another 30 min. After washed with KRP buffer once, cells were incubated in KRP containing 100 μmol·L^{-1} of 2-(*N*-(7-nitrobenz-2-oxa-1,3-diazol-4-yl) amino)-2-deoxyglucose (2-NBDG; Sigma-Aldrich) for 30 min. The intracellular amount of 2-NBDG was measured at an excitation wavelength of 475 nm and an emission wavelength of 550 nm. Glucose uptake was further normalized by protein content.

2.12 | Animals

All animal care and experimental procedures were in accordance with the guidelines and regulations and were approved by the Animal Ethical and Welfare Committee of University of Macau (No. ICMS-AEC-2015-07). Animal studies are reported in compliance with the ARRIVE guidelines (Kilkenny, Browne, Cuthill, Emerson, & Altman, 2010) and with the recommendations made by the *British Journal of Pharmacology*. Experimental protocols and design are reported in compliance with the guidelines (Curtis et al., 2018; Demirpence et al., 2016).

Male C57BL/6J mice (8–10 weeks old, RRID:IMSR_JAX:000664) were obtained from the Faculty of Health Science, University of Macau (Macau, China). The mice were housed at 22 ± 1°C with 12-hr light–dark cycles and fed with a regular chow diet (RD; Guangdong Medical Lab Animal Center, Guangzhou, Guangdong, China) and water ad libitum under standard conditions (specific-pathogen-free) with air filtration.

2.13 | Animal experimental procedure

Thirty-six C57BL/6J mice were randomly divided into six groups ($n = 6$). Two groups of mice were fed with an RD (calorie, 2.35 kcal·g^{-1}) and treated with PEG 400 solution (RD, 10 mL·kg^{-1} body weight, 30% in 0.9% saline) and the same volume of myricanol (RD + MY, 2.5 mg·mL^{-1} dissolved in PEG 400 solution), respectively. The other four groups of mice were fed with a 45% HFD (calorie, 4.5 kcal·g^{-1}, Trophic Animal Feed High-Tech Co., Nantong, Jiangsu, China) and treated with PEG 400 solution (HFD, 10 mL·kg^{-1} body weight, 30% in 0.9% saline), the same volume of low dosage of myricanol (MYL, 0.5 mg·mL^{-1} dissolved in PEG 400 solution), the same volume of high dosage of myricanol (MYH, 2.5 mg·mL^{-1} dissolved in PEG 400 solution), and the same volume of AICAR (5 mg·mL^{-1} dissolved in PEG 400 solution), respectively. The mice were intraperitoneally injected once a day for 18 weeks. Body weight and food intake were monitored every week. Twenty-four hours after the last injection, grip strength of each mouse was recorded using the Grip Strength Test Meter for Mice and Rats (Yiyan Science and Technology Development Co. Ltd, Zhejiang, China). Blood samples were collected from orbital sinus after deep anaesthesia with CO_2 suffocation and stored in a tube containing EDTA (1 mmol·L^{-1}). After centrifugation (1,200× *g*, 10 min, room temperature), serum was aliquoted and stored at −80°C. Mice were killed by CO_2 inhalation before dissection. The wet weights of epididymal fat, inguinal fat, brown adipose tissue (BAT), quadriceps, gastrocnemius, soleus, tibialis anterior, extensor digitorum longus, and liver were recorded, and the tissue indexes were calculated.

2.14 | Analysis of serum lipids

TG, total cholesterol, HDL cholesterol (HDL-C), and LDL cholesterol (LDL-C) levels in serum were analysed using commercial kits (Nanjing Jiancheng, Nanjing, Jiangsu, China), following the manufacturer's instruction.

2.15 | Metabolic characterizations

Metabolic parameters were obtained using an Oxymax open-circuit indirect calorimetry system (Columbus Instruments, Columbus, OH), as previously described (Lin et al., 2014). Briefly, mice were individually caged in chambers and given free access to indicated diet and water

for 1 week prior to tests. The first 24 hr in calorimetry chambers were considered the acclimation phase, and data were analysed only for the following 48 hr. Oxygen consumption and carbon dioxide production by each animal were measured.

2.16 | Glucose tolerance tests and insulin tolerance tests

Glucose tolerance test (GTT) and insulin tolerance test (ITT) were performed at 15 and 16 weeks post-treatment, respectively, as described previously (Shen et al., 2018). After 18-hr fasting, the tail blood glucose was measured using OneTouch Ultra blood glucose meter and LifeScan test strips. Then, the mice were received an intraperitoneal injection of glucose solution (Sigma-Aldrich) at a dose of 2.0 $g \cdot kg^{-1}$ body weight. The tail blood glucose was measured at 15, 30, 60, 90, and 120 min after injections. For the ITT, the tail blood glucose concentration was measured after 6-hr fasting. The mice were then received an intraperitoneal injection of human insulin (Eli Lilly, Indianapolis, IN, USA) at a dose of 1.0 $U \cdot kg^{-1}$ body weight. Tail blood glucose concentration was measured at 15, 30, 60, 90, and 120 min after injections. The constant rate for glucose disappearance (K_{ITT}) was calculated using the formula $0.0693 \cdot t_{1/2}{}^{-1}$. The half-time of glucose decay $t_{1/2}$ was calculated from the slope of the least square analysis of plasma glucose concentrations during the linear decay phase (Bonora et al., 1987). During GTT and ITT, blood samples were collected from the tail vein, after local anaesthesia with saline containing 2% lidocaine, to keep the animals comfortable.

2.17 | Homeostasis model assessment of basal insulin resistance

The homeostasis model assessment of basal insulin resistance (HOMA-IR) index was calculated as follows: fasting serum glucose·fasting serum insulin·22.5^{-1}, to assess insulin resistance. Lower HOMA-IR values indicated greater insulin sensitivity, whereas higher HOMA-IR values indicated insulin resistance.

2.18 | Analysis of TG and non-esterified free fatty acid levels in gastrocnemius muscle

TG and non-esterified free fatty acid (NEFA) levels in gastrocnemius muscle were analysed using commercial kits (Nanjing Jiancheng, Nanjing, Jiangsu, China), following the manufacturer's instruction. TG and NEFA levels were further normalized by protein content.

2.19 | Histological analysis of skeletal muscle and inguinal fat

A middle part of gastrocnemius muscle and inguinal fat were fixed in 4% paraformaldehyde overnight and then embedded into paraffin. Sections (4 μm thick) were used for haematoxylin and eosin (H&E) staining following the standard protocol.

2.20 | Microarray data mining strategy

To identify the differentially expressed genes (DEGs) in the process of browning of white adipose, gene expression data from microarray GSE8044 and GSE7032 (Seale et al., 2007; Timmons et al., 2007), showing transcriptomic profiles in BAT and WAT from C57BL/6J mice, were retrieved from the public Gene Expression Omnibus (GEO, RRID: SCR_005012) database. Next, differential gene expression level was calculated using GEO2R (RRID:SCR_016569), a tool combining GEOquery and limma R (RRID:SCR_010943) packages from Bioconductor project (RRID:SCR_006442; Davis & Meltzer, 2007). Meanwhile, the Gene Set Enrichment Analysis (GSEA) program was used to enrich the Gene Ontology biological process. The metric for ranking genes was set as "log2_Ratios_of_Classes," then heatmap was generated from the top 100 genes differentially expressed. A *P* value of .01 was used as the significance threshold that assessed by a Fisher's test corrected by Benjamini–Hochberg false discovery rate (FDR) method, which is the most commonly used adjustment for microarray data and provides a good balance between discovery of statistically significant genes and limitation of false positives (Benjamini & Yekutieli, 2001). To demonstrate potential protein–protein interaction networks, the candidate DEGs were mapped against the Search Tool for the Retrieval of Interacting Genes (STRING; RRID:SCR_005223) database version 10.5 (Szklarczyk et al., 2015). The network was constructed based on a medium confidence score of 0.4. The sub-cluster analysis was performed by *K*-means clustering.

2.21 | Real-time quantitative RT-PCR

Total RNA was isolated from inguinal adipose tissue using TRIzol Reagent (Invitrogen), following the manufacturer's instructions. The cDNA was synthesized from 1-μg RNA using the SuperScript III First-Strand Synthesis System (Invitrogen). The real-time quantitative PCR (qPCR) experiments were conducted on Step-One plus real-time PCR System using SYBR Green PCR Master Mix (Thermo Scientific) with gene specific primers (Table S2). *18S* RNA was used as an internal control.

2.22 | Data and statistical analysis

The data and statistical analysis comply with the recommendations of the *British Journal of Pharmacology* on experimental design and analysis in pharmacology. The authors declare that the data supporting the findings of this study are available within the article. Studies were designed to generate groups of equal size, and no data points were excluded from the analysis in any experiment. The *n* value for each experiment was shown in the figure legend. This was based on our previous results (Shen, Liao, Liu, et al., 2019; Shen, Liao, Feng, et al., 2019) and also for the purpose of carrying out statistical analysis according to the guidelines of *British Journal of Pharmacology* (Curtis et al., 2018). Cells and mice were randomly assigned to each treatment group and experiment. All the quantifications and data analysis were blinded, and the analyst did not know the origin of the data during

statistical analysis. Data normalization was undertaken to control for sources of variation of baseline parameters and to allow comparison of the magnitude of drug effects in different conditions. The units of a variable were determined as fold mean of the controls. All data were expressed as mean ± SD and analysed by Graphpad Prism 7 (RRID: SCR_002798, GraphPad Software, San Diego, CA, USA). Statistical analysis was undertaken only for studies where each group size was at least $n = 5$. The declared group size is the number of independent values and that statistical analysis was carried out using these independent values. Statistical analysis of differences between two treatment groups was performed using an independent samples t test. For multiple comparisons, one-way or two-way ANOVA with Bonferroni's correction was applied. The post hoc tests were run only if F achieved $P < .05$ and there was no significant variance inhomogeneity. The one-way ANOVA was used for statistical comparison, and P values less than .05 were considered statistically significant.

2.23 | Materials

Myricanol was isolated from the bark of *M. rubra* as described previously (Shen, Liao, Feng, et al., 2019). AICAR was purchased from Selleck Chemicals (Houston, TX, USA). PBS powder, DMEM, P/S, FBS, and horse serum were purchased from Gibco (Grand Island, NY, USA). Calf serum was obtained from HyClone (Logan, UT, USA). **Compound C (dorsomorphin)**, IBMX, dexamethasone, insulin, and PA were obtained from Sigma-Aldrich (St. Louis, MO, USA). Antibodies against p-ACC (RRID:AB_330337), **ACC** (RRID:AB_2219400), PGC-1α (RRID:

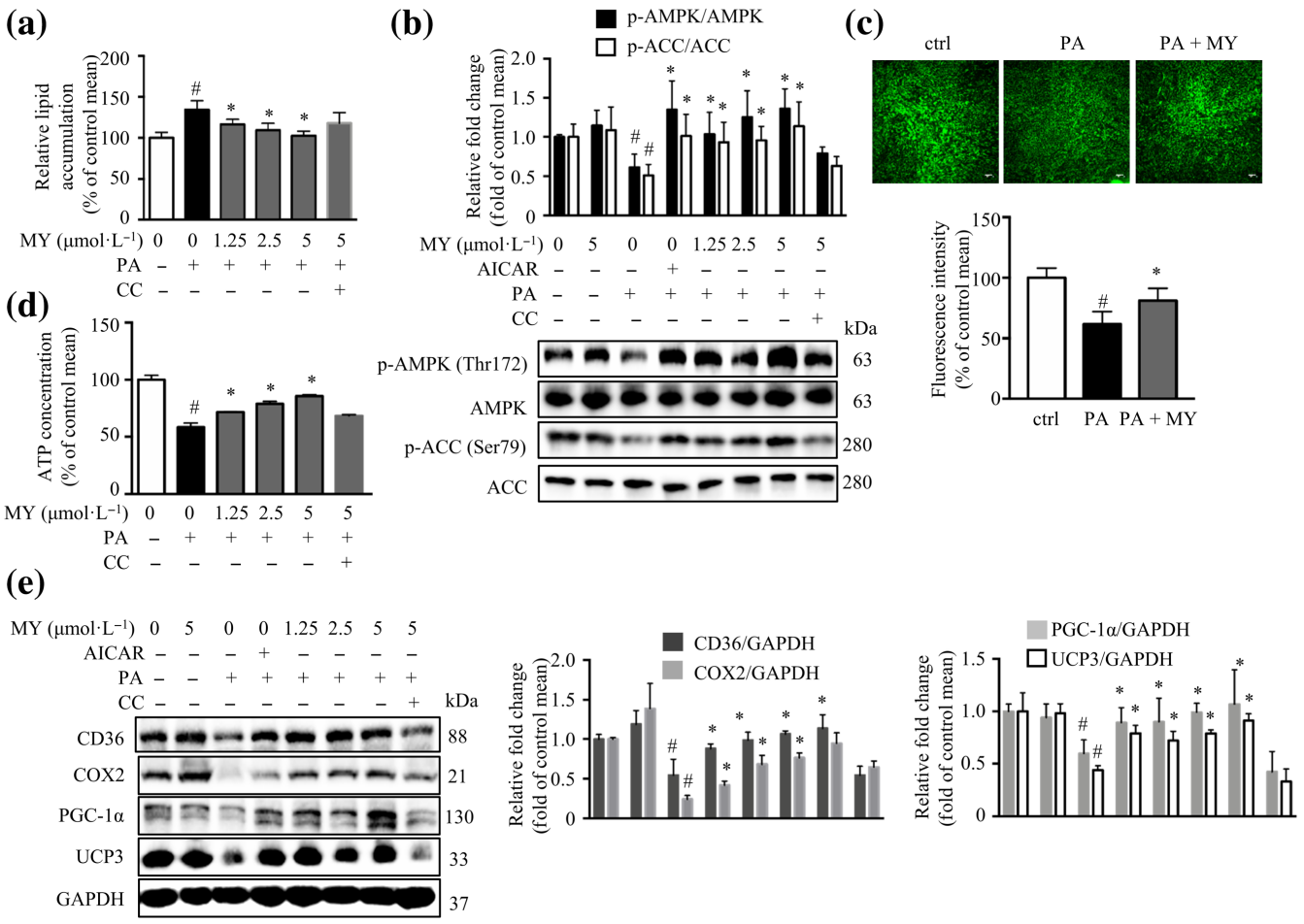

FIGURE 1 Myricanol (MY) decreases lipid accumulation and enhances mitochondrial content in palmitic acid (PA)-treated C2C12 myotubes. C2C12 myotubes were treated with DMSO as a vehicle control, AICAR (20 μmol·L^{-1}) as a positive control, Compound C (CC; 10 μmol·L^{-1}), or different concentrations of myricanol (1.25, 2.5, and 5 μmol·L^{-1}) for 24 hr. (a) Myricanol dose-dependently reduced lipid accumulation in PA-treated C2C12 myotubes, assessed by Nile red staining ($n = 6$). (b) Myricanol increased the phosphorylation of ACC and AMPK in PA-treated C2C12 myotubes ($n = 6$). (c) Myricanol increased mitochondrial content in PA-treated C2C12 myotubes, assessed by MitoTracker Green staining and flow cytometry ($n = 6$). Scale bar = 100 μm. (d) Myricanol promoted ATP production in a dose-dependent manner in PA-treated C2C12 myotubes ($n = 6$). (e) Myricanol increased the expression levels of CD36, COX2, PGC-1α, and UCP3. GAPDH was used as a loading control ($n = 6$). Data are shown as mean ± SD. $^{*}P < .05$, MY significantly different from PA-treated cells $^{\#}P < .05$, ctrl cells significantly different from PA-treated cells. Differences between two treatment groups were assessed using one-way ANOVA followed by independent-samples' t-test. For multiple comparisons, one-way or two-way ANOVA with Bonferroni's correction was applied

AB_823600), insulin receptor substrate 1 (**IRS1**; RRID:AB_330333), p-GSK3β (RRID:AB_2115201), and **GSK3β** (RRID:AB_2636978) were obtained from Cell Signaling Technology (Beverly, MA, USA). Antibodies against p-AMPK (RRID:AB_2169714), AMPK (RRID:AB_2169546), CD36; RRID:AB_2072518), cytochrome *c* oxidase subunit II (**COX2**; RRID:AB_2066365), **UCP3** (RRID:AB_2213920), PPARγ (RRID:AB_654710), p-Akt (RRID:AB_667741), **Akt** (RRID:AB_671714), UCP1 (RRID:AB_2213781), p-IRS1 (RRID:AB_669445), β-actin (RRID:AB_630836), and GAPDH (RRID:AB_10167668) were obtained from Santa Cruz Biotechnology (Santa Cruz, CA, USA). Antibodies against irisin and **SIRT1** were obtained from Proteintech (Rosemont, IL, USA). All other chemicals (analytical grade) unless specified were obtained from Sigma-Aldrich (St. Louis, MO, USA). ELISA kit for insulin was obtained from Mercodia (Uppsala, Sweden). ELISA kit for irisin was obtained from Aviscera Bioscience (Santa Clara, CA, USA). Oligonucleotide primers, SuperScript III First-Strand Synthesis System, and TRIzol Reagent were purchased from Invitrogen (Carlsbad, CA, USA). BCA protein assay kit, SYBR Green PCR Master Mix, SuperSignal West Femto Maximum Sensitivity Substrate were obtained from Thermo Fisher Scientific (Grand Island, NY, USA).

2.24 | Nomenclature of targets and ligands

Key protein targets and ligands in this article are hyperlinked to corresponding entries in http://www.guidetopharmacology.org, the common portal for data from the IUPHAR/BPS Guide to PHARMACOLOGY (Harding et al., 2018), and are permanently archived in the Concise Guide to PHARMACOLOGY 2017/18 (Alexander, Cidlowski et al., 2017; Alexander, Fabbro et al., 2017; Alexander, Kelly et al., 2017).

3 | RESULTS

3.1 | Myricanol decreases lipid accumulation and enhances mitochondrial function in PA-treated C2C12 myotubes

When treated with 250 μmol·L^{-1} of PA for 24 hr, the C2C12 myotubes accumulated around 40% more lipid compared with the control cells, without obvious cytotoxicity (Figure S1a–c). Thus, C2C12 myotubes were treated with 250 μmol·L^{-1} of PA for 24 hr in the following experiments. myricanol did not exhibit obvious cytotoxicity in C2C12 myotubes up to 5 μmol·L^{-1} (Figure S1d,e) but decreased PA-induced lipid accumulation in a dose-dependent manner (Figure 1a). Our previous study showed that myricanol acts as an AMPK activator in adipocytes (Shen, Liao, Feng, et al., 2019). Indeed, myricanol activated AMPK and increased the phosphorylation of **acetyl-CoA carboxylase (ACC)**, a substrate of AMPK, in PA-treated C2C12 myotubes, as potently as the known AMPK activator, AICAR (Figure 1b). To confirm that the effect of myricanol on lipid accumulation is through activating AMPK, C2C12 myotubes were treated with an AMPK inhibitor, Compound C, together with myricanol. When co-treated with Compound C, the effects of myricanol on lipid accumulation and the phosphorylation of AMPK and ACC were almost abolished (Figure 1a,b).

PA-induced lipid accumulation is accompanied with mitochondrial dysfunction. The MitoTracker Green staining showed that myricanol reversed PA-induced loss of mitochondrial content (Figure 1c) and decrease of ATP content (Figure 1d). Myricanol elevated the expression levels of the master regulator of mitochondrial biogenesis–PGC-1α, the fatty acid translocase protein–CD36, and the mitochondrial markers–COX2 and UCP3, which were almost abolished by the co-treatment with Compound C (Figure 1e).

In a further series of experiments, an *Apmka1* silenced C2C12 cell line (si*Ampka1*) was generated. The si*Ampka1* cells expressed about 60% less AMPKα1 protein compared with that in the cells expressing scrambled siRNA (scrambled; Figure 2a). Myricanol did not reverse PA-induced lipid accumulation in si*Ampka1* cells (Figure 2b). Moreover, myricanol rescued PA-induced reduction of mitochondrial content in the scrambled cells but not in si*Ampka1* cells, assessed by Mitotracker Green staining (Figure 2c) and citrate synthase activity (Figure 2d). Next, the Seahorse assay results indicated that PA-treated myotubes exhibited reduced mitochondrial respiration under basal and FCCP-stimulated condition, whereas myricanol treatment reversed PA-induced suppression of OCR (Figure 2e). Myricanol also enhanced glycolysis in PA-treated myotubes as indicated by the higher ECAR (Figure 2e). However, the effects of myricanol on OCR and ECAR were abolished in si*Ampka1* cells (Figure 2e). Taken together, these results showed that myricanol decreased lipid accumulation by enhancing mitochondrial content and function in PA-treated C2C12 myotubes, which was mediated through activating AMPK.

3.2 | Myricanol protects C2C12 myotubes against PA-induced insulin resistance

Myricanol reduced PA-induced lipid accumulation in C2C12 myotubes, which might in turn enhance insulin sensitivity. We evaluated insulin-stimulated glucose uptake in C2C12 myotubes. In normal myotubes, myricanol (5 μmol·L^{-1}) treatment increased insulin-stimulated glucose uptake by 35.5%, compared with the vehicle cells (Figure 3a). As expected, PA treatment dramatically suppressed insulin-stimulated glucose uptake by 52.0%, compared with the normal cells, while myricanol dose-dependently enhanced insulin-stimulated glucose uptake in PA-treated cells (Figure 3a). Interestingly, when co-treated with Compound C, the insulin sensitizing effect of myricanol was partly blocked (Figure 3a). PA treatment reduced insulin-stimulated phosphorylation of IRS1, **Akt**, and glycogen synthase kinase 3β (GSK3β), when compared with those of normal cells, whereas myricanol treatment (5 μmol·L^{-1}) dramatically increased the phosphorylation of IRS1, Akt, and GSK3β in PA-treated C2C12 cells (Figure 3b). As expected, the effect of myricanol in enhancing insulin-stimulated glucose uptake was partially abolished in si*Ampka1* myotubes (Figure 3c). Thus, myricanol protected C2C12 myotubes against PA-induced insulin resistance through activating AMPK.

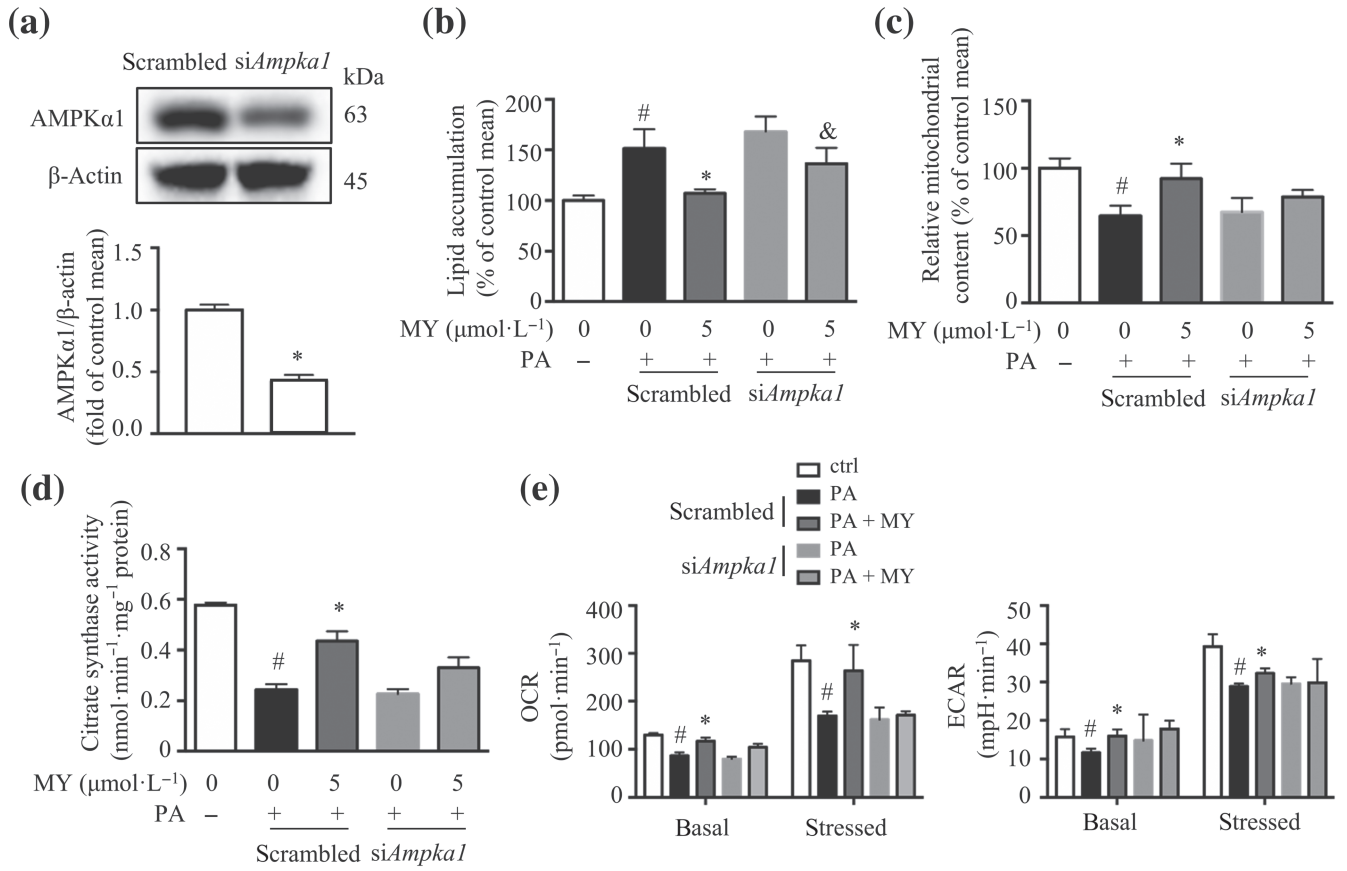

FIGURE 2 Myricanol (MY) protects C2C12 myotubes against palmitic acid (PA)-induced lipid accumulation and mitochondrial dysfunction via activating AMPK. (a) AMPKα1 expression in si*Ampka1* and scrambled cells was determined by Western blot. β-Actin was used as a loading control ($n = 6$). $^{*}P < .05$, si*Ampka1* significantly different from scrambled. (b) Lipid accumulation in PA-treated scrambled and si*Ampka1* cells, assessed by Nile red staining ($n = 6$). (c) Mitochondrial content in PA-treated scrambled and si*Ampka1* cells, assessed by MitoTracker Green staining and flow cytometry ($n = 6$). (d) Citrate synthase activity in PA-treated scrambled and si*Ampka1* cells. (e) Oxygen consumption rate (OCR) and extracellular acidification rate (ECAR) in PA-treated scrambled and si*Ampka1* cells, assessed by Seahorse assay ($n = 6$). Data are shown as mean ± SD. $^{*}P < .05$, MY significantly different from PA-treated cells $^{\#}P < .05$, ctrl cells significantly different from PA-treated cells. $^{\&}P < .05$, si*Ampka1* significantly different from scrambled. Differences between two treatment groups were assessed using one-way ANOVA followed by independent-samples' t-test. For multiple comparisons, one-way or two-way ANOVA with Bonferroni's correction was applied

3.3 | Myricanol stimulates the secretion of irisin to induce the browning of 3T3-L1 adipocytes

Irisin is a PGC-1-induced myokine secreted from skeletal muscle following exercise, which induces the browning of WAT (Boström et al., 2012). Indeed, PA treatment suppressed irisin protein level, whereas myricanol treatment led to an increase of irisin protein level in PA-treated C2C12 myotubes, which was reversed by the co-treatment with Compound C (Figure 4a). Moreover, the ELISA results showed that myricanol treatment increased the production of irisin in C2C12 myotubes lysates and the secretion of irisin in culture medium, which were partly reversed by Compound C (Figure 4b,c).

Next, the mature 3T3-L1 adipocytes were incubated with CM from C2C12 myotubes treated with different concentrations of myricanol (Figure S2). The Oil Red O staining and Nile red staining results revealed that CM from myricanol-treated myotubes decreased the lipid accumulation in 3T3-L1 adipocytes in a dose-dependent manner, as well as the CM from AICAR-treated myotubes (Figure 4d). CM from myricanol-treated myotubes also reduced TG accumulation in 3T3-L1 cells in a dose-dependent manner (Figure 4e). Incubation with the CM from myricanol-treated myotubes increased the browning markers, PGC-1α and UCP1, and the mitochondrial marker, COX2, and suppressed the adipogenic marker, PPARγ, in 3T3-L1 adipocytes, dose-dependently (Figure 4f).

To confirm that the browning effect of myricanol was mediated through irisin, an *Fndc5* silenced C2C12 cell line (si*Fndc5*) was generated. The si*Fndc5* cell line expressed about 55% less irisin protein compared with that of the cells expressing scrambled siRNA (scrambled; Figure 4g). The CM from si*Fndc5* cells did not affect TG content but significantly decreased the expression of PGC-1α, UCP1, and COX2 and increased the expression of PPARγ in 3T3-L1 adipocytes, compared with those from scrambled cells (Figure 4h,i). The CM from myricanol-treated si*Fndc5* cells did not change the TG content or the expression levels of PGC-1α, UCP1, COX2, and PPARγ, in 3T3-L1 adipocytes (Figure 4h,i).

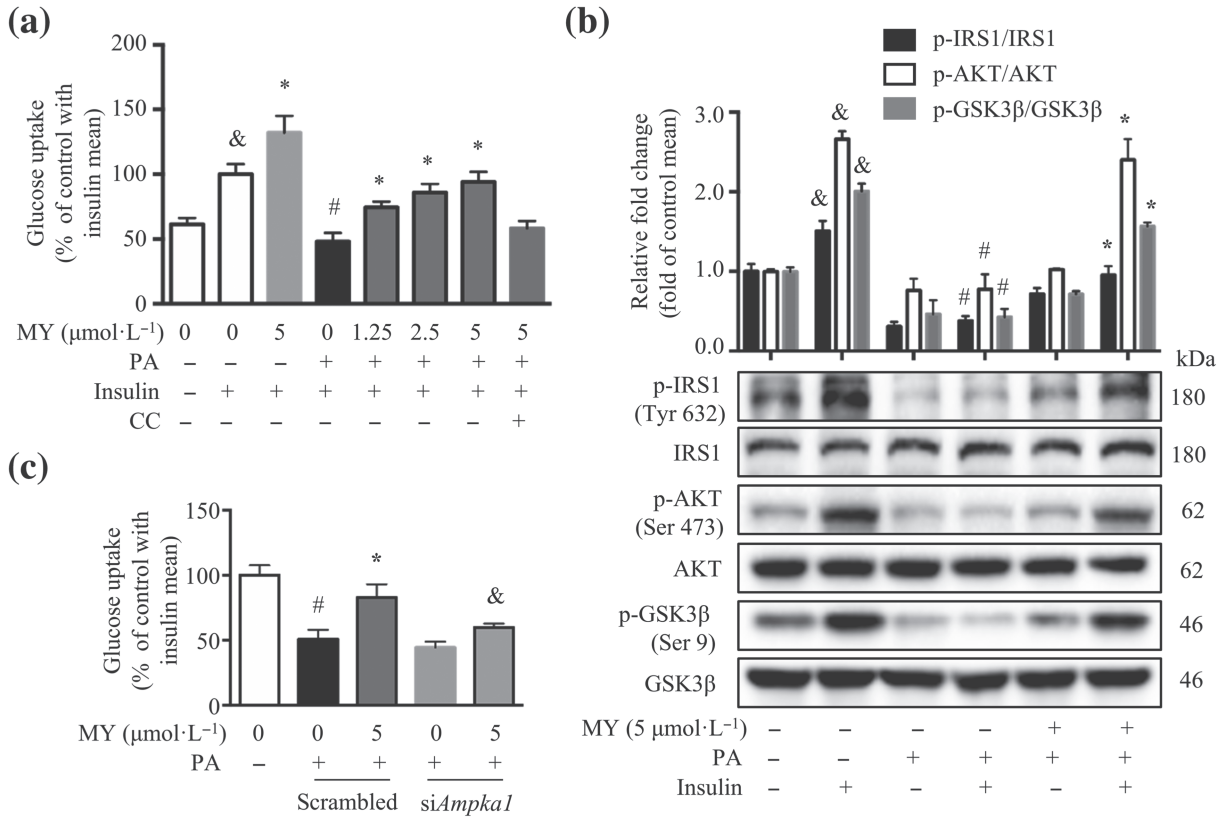

FIGURE 3 Myricanol (MY) protects C2C12 myotubes against palmitic acid (PA)-induced insulin resistance. (a) Myricanol promoted insulin-stimulated glucose uptake in PA-induced C2C12 myotubes ($n = 6$). (b) Myricanol activated the insulin signalling pathway in PA-treated C2C12 myotubes. The expression of p-IRS-1, IRS-1, p-Akt, Akt, p-GSK3β, and GSK3β was analysed by Western blot. ($n = 6$). Data are shown as mean ± SD. $^{\&}P < .05$, with insulin significantly different from without insulin. $^{\#}P < .05$, ctrl cells with insulin significantly different from PA-treated cells with insulin. $^{*}P < .05$, MY significantly different from PA-treated cells. (c) Insulin-stimulated glucose uptake in PA-treated scrambled and si*Ampka1* cells. ($n = 6$). Data are shown as mean ± SD. $^{*}P < .05$, MY significantly different from PA-treated cells. $^{\#}P < .05$, ctrl cells significantly different from PA-treated cells. $^{\&}P < .05$, si*Ampka1* significantly different from scrambled. Differences between two treatment groups were assessed using one-way ANOVA followed by independent-samples' t-test. For multiple comparisons, one-way or two-way ANOVA with Bonferroni's correction was applied

The browning of adipocytes is always associated with an increase of oxygen consumption (Altshuler-Keylin & Kajimura, 2017). UCP1 is required to dissipate chemical energy as heat through thermogenic respiration in brown adipocytes and beige cells. GDP, a classic UCP1 inhibitor, was used to evaluate the role of myricanol in inducing browning of 3T3-L1 adipocytes (Fedorenko, Lishko, & Kirichok, 2012). The basal and stressed OCRs and ECARs of the 3T3-L1 adipocytes were enhanced when incubated with the CM from myricanol- or AICAR-treated myotubes, which were abolished by incubation with the CM from MY- and GDP-co-treated myotubes (Figure 4j). The above results suggested that myricanol increased irisin production and secretion in myotubes, which in turn induced the browning of adipocytes.

3.4 | Myricanol retards fat mass gain and improves lipid profiles in HFD-fed mice

To evaluate the role of myricanol in improving metabolic disorders, HFD-induced obese and insulin-resistant mice were recruited (Figure S3). AICAR (50 mg·kg^{-1}) was used as a positive control. Eighteen weeks of HFD feeding induced more body weight gain than RD feeding (Figure 5a). Analysis with two-way ANOVA showed a significant effect of time and of treatment, along with a significant interaction (time x treatment). Either low dose (MYL) or high dose (MYH) treatment with myricanol reduced the body weight gain under HFD feeding, which was comparable with the AICAR treatment (Figure 5a). The MYH treatment (25 mg·kg^{-1} day^{-1}) in RD-fed mice did not change the body weight (Figure 5a). Food intake was unchanged in myricanol-treated mice (Figure 5b). The grip strength test indicated that HFD-fed mice decreased nearly 20% muscle strength compared with RD-fed mice, whereas myricanol treatment protected the mice against HFD-induced muscle weakness (Figure 5c). The indirect calorimetry data showed that HFD-fed mice exhibited lower oxygen consumption than that of RD-fed mice in both light and dark periods, whereas myricanol treatment clearly enhanced oxygen consumption (Figure 5d). The body weight gain of HFD-fed mice was accompanied by a notable fat accumulation, including visceral epididymal fat and subcutaneous inguinal fat but not liver or BAT, when compared with RD-fed mice (Figures 5e and S4a,b). In contrast, myricanol treatment markedly decreased

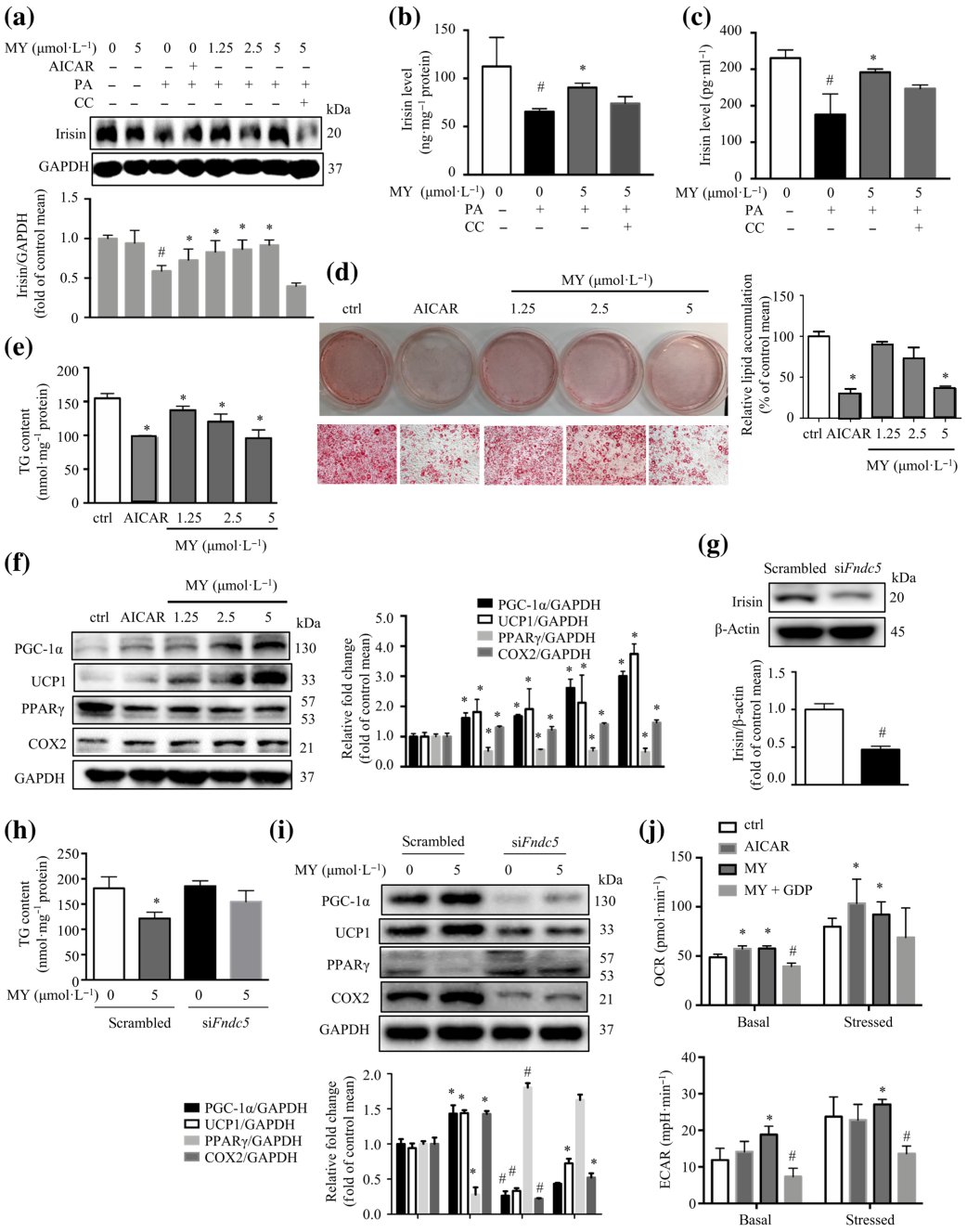

FIGURE 4 Myricanol (MY) stimulates irisin secretion to induce the browning of 3T3-L1 adipocytes. (a) Myricanol increased the protein expression of irisin. GAPDH was used as a loading control. Myricanol led to an increase of (b) irisin production in C2C12 myotubes lysates (n = 6) and (c) irisin secretion in C2C12 myotubes culture medium (n = 6), determined by ELISA kit. (d) 3T3-L1 adipocytes were co-cultured with conditioned media (CM) from C2C12 myotubes for 24 hr, and the lipid content was determined by Oil Red O staining and Nile red staining (n = 6). Scale bar = 100 μm. (e) Triglyceride (TG) content in 3T3-L1 was determined. (n = 6). (f) The expression of PGC-1α, UCP1, PPARγ, and COX2 in 3T3-L1 adipocytes was assessed by Western blot (n = 6). GAPDH was used as a loading control. Data are shown as mean ± SD. $^{\#}P < .05$, ctrl cells significantly different from palmitic acid (PA)-treated cells. $^{*}P < .05$, MY/AICAR significantly different from PA-treated cells. (g) Irisin expression in si*Fndc5* and scrambled cells was determined by Western blot (n = 6). β-Actin was used as a loading control. 3T3-L1 adipocytes were co-cultured with CM from si*Fndc5* and scrambled cells for 24 hr. (h) TG content in 3T3-L1 was determined. (n = 6). (i) The expression of PGC-1α, UCP1, PPARγ, and COX2 in 3T3-L1 adipocytes was assessed by Western blot (n = 6). GAPDH was used as a loading control. Data are shown as mean ± SD. $^{\#}P < .05$, si*Fndc5* significantly different from scrambled. $^{*}P < .05$, MY significantly different from PA-treated cells. (j) 3T3-L1 adipocytes were cultured with CM from DMSO, AICAR, or MY-treated C2C12 myotubes, or CM from MY-treated C2C12 myotubes together with 100 μmol·L^{-1} of GDP, for 24 hr. The oxygen consumption rate and extracellular acidification rate in 3T3-L1 adipocytes were assessed by Seahorse assay (n = 6). Data are shown as mean ± SD. $^{*}P < .05$, MY/AICAR significantly different from PA-treated cells. $^{\#}P < .05$, MY + GDP significantly different from MY alone. Differences between two treatment groups were assessed using one-way ANOVA followed by independent-samples' t-test. For multiple comparisons, one-way or two-way ANOVA with Bonferroni's correction was applied

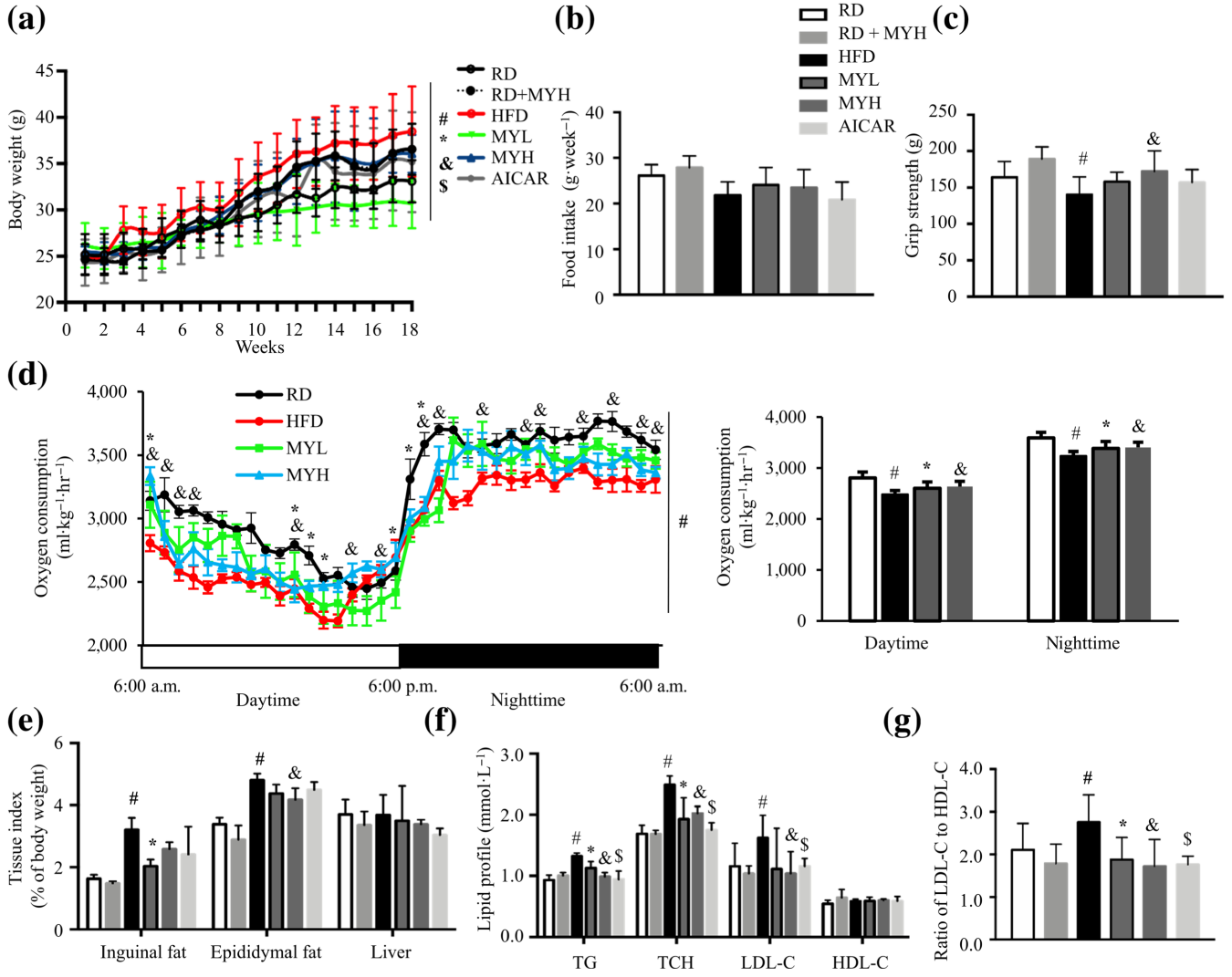

FIGURE 5 Myricanol (MY) retards fat mass gain and improves lipid profile in high-fat diet (HFD)-fed mice. (a) Body weight of mice under regular chow diet (RD) or HFD feeding ($n = 6$). There was a significant effect of time, $F(17, 48) = 119.4$; of treatment, $F(5, 24) = 1.844$; and interaction, $F(85, 408) = 1.764$; two-way ANOVA. (b) Weekly food intake of mice ($n = 6$). (c) Grip strength of mice ($n = 6$). (d) Oxygen consumption of mice during light and dark cycles ($n = 6$). (e) Tissue index of mice ($n = 6$). (f) Triglyceride (TG), total cholesterol (TCH), LDL cholesterol (LDL-C), and HDL cholesterol (HDL-C) in serum ($n = 6$). (g) The ratio of LDL-C to HDL-C ($n = 6$). Data are shown as mean ± SD. $^{*}P < .05$, low dose myricanol (MYL) significantly different from HFD. $^{\&}P < .05$, high dose myricanol (MYH) significantly different from HFD or RD significantly different from RD + MYH. $^{\#}P < .05$, RD significantly different from HFD. $^{\$}P < .05$, AICAR significantly different from HFD. Differences between two treatment groups were assessed using one-way ANOVA followed by independent-samples' t-test. For multiple comparisons, one-way or two-way ANOVA with Bonferroni's correction was applied

the ratios of epididymal fat and inguinal fat but not liver or BAT, compared with HFD-fed mice (Figures 5e and S4a,b). Notably, the MYL, but not the MYH, treatment reversed HFD-induced decrease of the ratios of quadriceps, gastrocnemius, and tibialis anterior (Figure S4c,d). The above data indicated that myricanol treatment protected mice from HFD-induced body weight gain, fat accumulation, and muscle weakness.

Next, the lipid profile in serum was evaluated. HFD feeding increased serum levels of TG, total cholesterol, and LDL-C but not HDL-C, whereas either MYL or MYH treatment greatly improved lipid profile (Figure 5f). The ratio between detrimental LDL-C and beneficial HDL-C was increased in HFD-fed mice, which was reversed by myricanol treatment (Figure 5g). Thus, myricanol alleviated HFD-induced hyperlipidaemia.

3.5 | Myricanol improves insulin sensitivity in HFD-fed mice

During GTT, the glucose clearance rate was greatly interrupted in HFD-fed mice, and either MYL or MYH treatment clearly improved glucose disposal rate, similar to that of RD-fed mice and AICAR-treated mice (Figure 6a). In ITT experiments, the glucose levels of myricanol-treated mice were significantly reduced under insulin

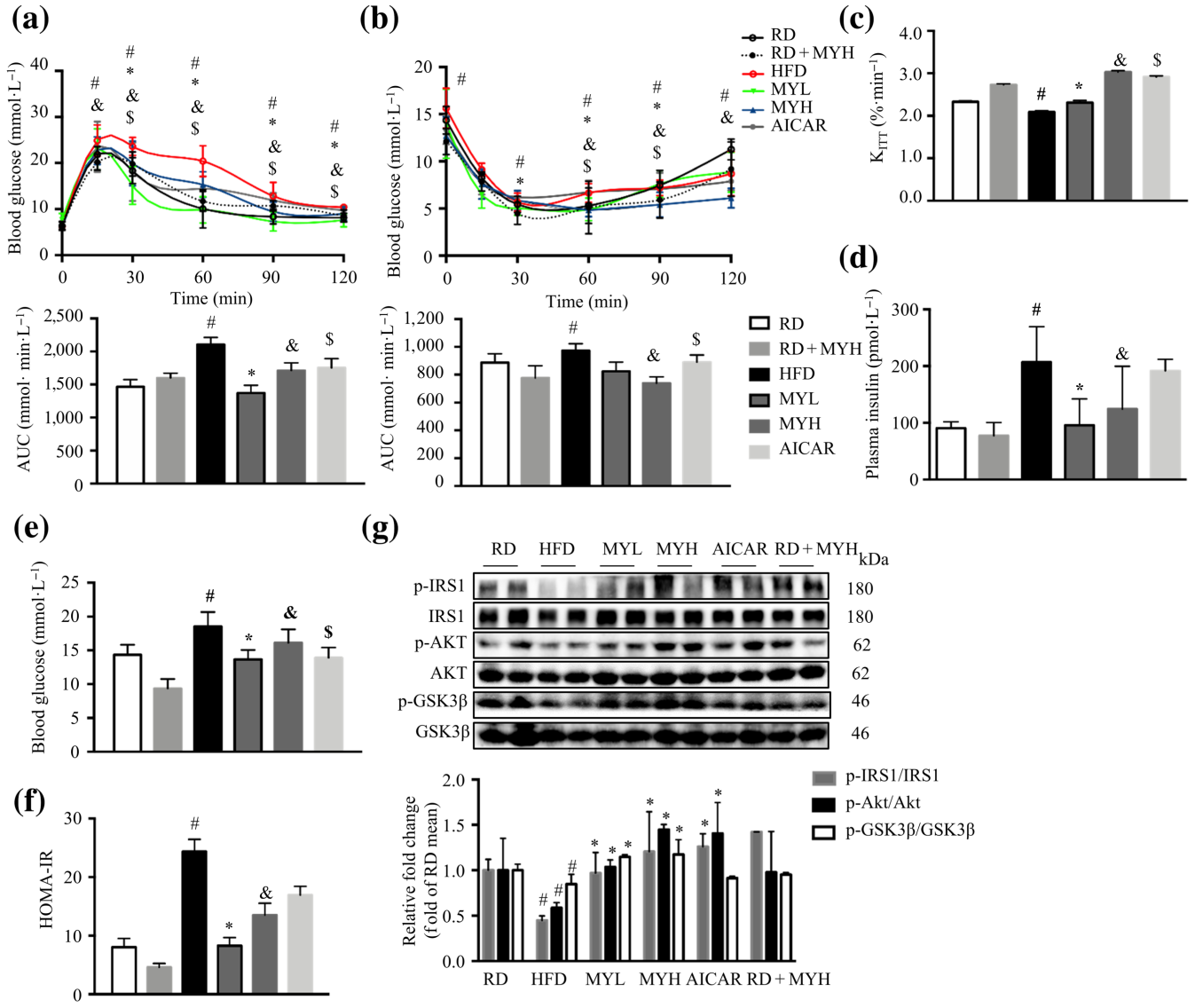

FIGURE 6 Myricanol (MY) improves insulin sensitivity in high-fat diet (HFD)-fed mice. (a) Glucose tolerance test was performed after 15-week myricanol treatment. AUC of each group was calculated (n = 6). (b) ITT was performed after 16-week myricanol treatment. AUC of each group was calculated (n = 6). (c) K_{ITT} of mice. The serum levels of (d) insulin and (e) glucose were determined after 18-hr fasting (n = 6). (f) The homeostasis model assessment of basal insulin resistance (HOMA-IR) of mice. (g) The expression of key proteins in insulin signalling pathway in gastrocnemius muscle, including p-IRS1, IRS1, p-Akt, Akt, p-GSK3β, and GSK3β, was determined by Western blot (n = 6). Data are shown as mean ± SD. $^{*}P < .05$, low dose myricanol (MYL) significantly different from HFD. $^{\&}P < .05$, high dose myricanol (MYH) significantly different from HFD or regular chow diet (RD) significantly different from RD + MYH. $^{\#}P < .05$, RD significantly different from HFD. $^{\$}P < .05$, AICAR significantly different from HFD. Differences between two treatment groups were assessed using one-way ANOVA followed by independent-samples' t-test. For multiple comparisons, one-way or two-way ANOVA with Bonferroni's correction was applied

stimulation, as low as those of RD-fed mice (Figure 6b). Furthermore, the constant rate for glucose disappearance (K_{ITT}) was calculated. The results showed that HFD feeding induced significant reduction of K_{ITT}, which was restored by myricanol treatment (Figure 6c). In both GTT and ITT, myricanol exhibited no obvious effect on RD-fed mice (Figure 6a,b).

Furthermore, the fasting insulin level was almost doubled in HFD-fed mice in comparison with RD-fed mice, whereas the fasting insulin levels in mice from the MYL and MYH groups were around 50% lower than that of the HFD-fed mice (Figure 6d). Similarly, myricanol treatment significantly reduced the fasting glucose levels in HFD-fed mice (Figure 6e). HOMA-IR calculation indicated that either MYL or MYH markedly improved insulin sensitivity in HFD-fed mice, which was comparable with that of RD-fed group (Figure 6f). HFD feeding suppressed the phosphorylation of IRS-1, AKT, and GSK-3β, while myricanol treatment dose-dependently reversed the above changes (Figure 6g). Taken together, these data showed that myricanol treatment effectively alleviated HFD-induced insulin resistance.

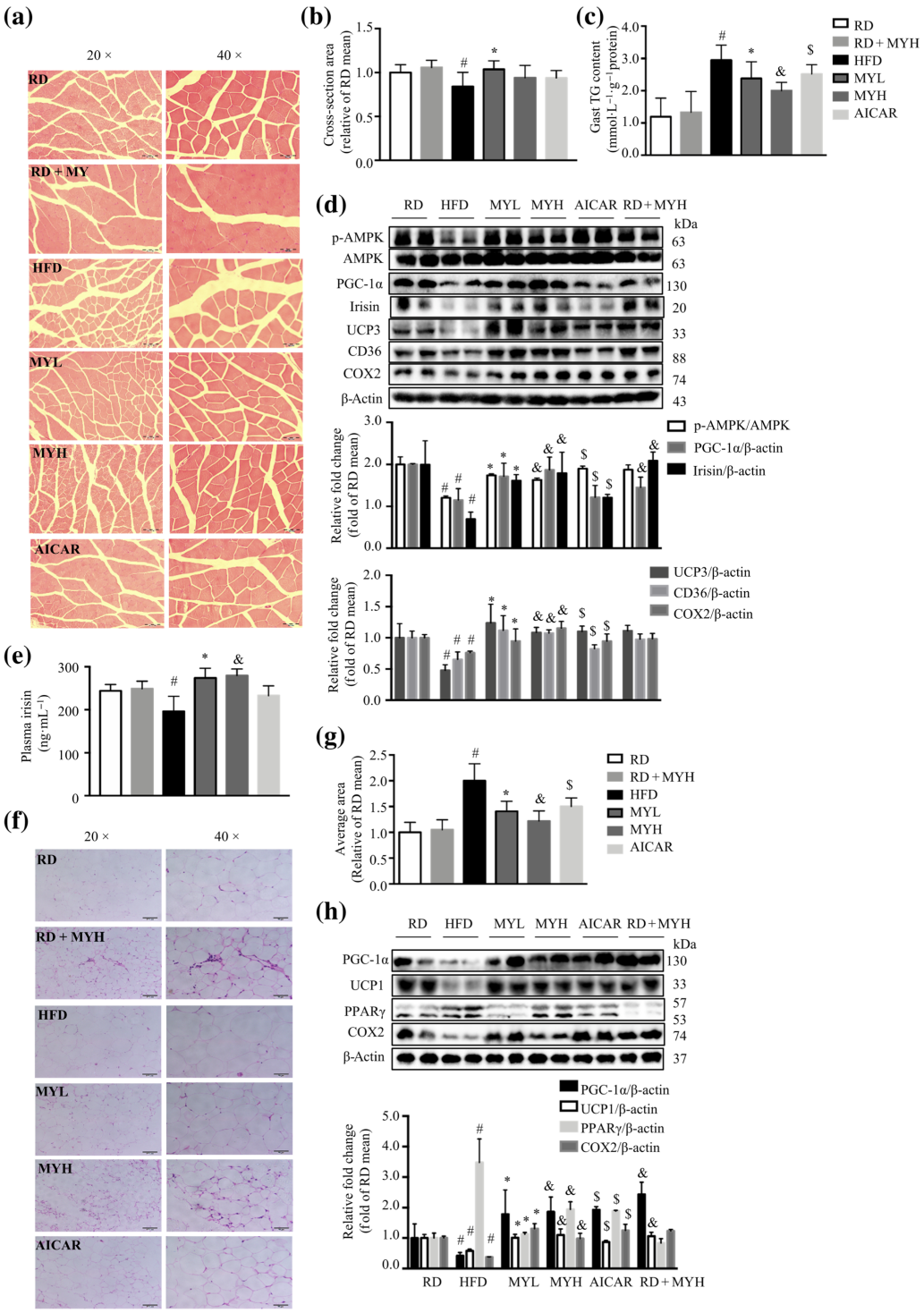

FIGURE 7 Myricanol (MY) enhances irisin secretion to induce the browning of inguinal fat. (a) Representative haematoxylin and eosin staining of myofibre cross section of gastrocnemius muscle (Gast; $n = 5$). Scale bar = 100 μm on the left; scale bar = 50 μm on the right. (b) Skeletal muscle fibre diameter ($n = 5$). (c) Triglyceride (TG) level in gastrocnemius muscle ($n = 6$). (d) The expression of p-AMPK, AMPK, PGC-1α, irisin, UCP3, CD36, and COX2 in gastrocnemius muscle was assessed by Western blot ($n = 6$). β-Actin was used as a loading control. (e) The serum level of irisin was determined by ELISA kit ($n = 6$). (f) Representative haematoxylin and eosin staining of inguinal white adipose tissue (WAT; $n = 5$). Scale bar = 100 μm on the left; scale bar = 50 μm on the right. (g) Adipocyte diameter in inguinal WAT ($n = 5$). (h) The expression levels of PGC-1α, UCP1, PPARγ, and COX2 in inguinal WAT were determined by Western blot. β-Actin was used as a loading control ($n = 6$). Data are shown as mean ± SD. $^{*}P < .05$, low dose myricanol (MYL) significantly different from high-fat diet (HFD). $^{\&}P < .05$, high dose myricanol (MYH) significantly different from HFD or regular chow diet (RD) significantly different from RD + MYH. $^{\#}P < .05$, RD significantly different from HFD. $^{\$}P < .05$, AICAR significantly different from HFD. Differences between two treatment groups were assessed using one-way ANOVA followed by independent-samples' t-test. For multiple comparisons, one-way or two-way ANOVA with Bonferroni's correction was applied

3.6 | Myricanol enhances irisin secretion to induce the browning of inguinal fat

HFD-induced obesity and insulin resistance are associated with mitochondrial dysfunction and intramyocellular lipid accumulation (Koves et al., 2008). The H&E staining of gastrocnemius muscle was performed to better characterize the effect of myricanol on muscle morphology. The skeletal muscle from RD-fed mice exhibited normal architecture with dense appearance fibres, whereas that from HFD-fed mice showed degenerative changes in muscle myofibres. In contrast, myricanol treatment retained normal architecture in muscle myofibres, similar to that of RD-fed mice (Figure 7a). The cross-sectional area of muscle fibre in HFD-fed mice was decreased about 20% compared with that of RD-fed mice, whereas myricanol treatment prevented HFD-induced atrophy of muscle fibre (Figure 7b). As shown in Figure 7c, HFD feeding induced TG accumulation in gastrocnemius muscle; either MYH or MYL treatment greatly alleviated HFD-induced TG deposition in skeletal muscle. The NEFA level was unchanged in HFD-fed mice, with or without myricanol administration (Figure S4e). The expression levels of PGC-1α, COX2, CD36, and UCP3, as well as the phosphorylation level of AMPK, were significantly decreased in muscle from HFD-fed mice, indicating mitochondrial dysfunction, whereas myricanol treatment totally reversed the above changes, resulting in enhanced mitochondrial biogenesis and function (Figure 7d). These results indicated that myricanol prevented the HFD-induced muscle dysfunction, by enhancing mitochondrial function and attenuating intramyocellular lipid accumulation.

Interestingly, myricanol treatment led to a significant increase of irisin expression in gastrocnemius muscle from mice under HFD feeding (Figure 7d). Moreover, the serum irisin level in HFD-fed mice was lower than that in the RD-fed mice, while myricanol treatment markedly increased the circulating irisin level (Figure 7e). Next, H&E staining of inguinal fat revealed that the average adipocyte diameter of HFD-fed mice was twice that of RD-fed mice, and myricanol treatment decreased the diameter of adipocytes by nearly 35% (Figure 7f, g). Moreover, the inguinal fat from MY-treated mice showed the appearance of multiocular adipocytes, a characteristic of brown adipocytes, suggesting that myricanol might induce brown-like remodelling of inguinal fat (Figure 7f). The protein levels of UCP1, PGC-1α, and COX2 were suppressed, and the protein level of PPARγ was increased in inguinal fat from HFD-fed mice (Figure 7h). Myricanol treatment increased the protein expression of UCP1, PGC-1α, and COX2 while decreased the expression of PPARγ in inguinal fat (Figure 7h). Myricanol treatment also reversed HFD-induced down-regulation of UCP1 and PGC-1α in BAT (Figure S4f). Collectively, these results suggested that myricanol stimulated the secretion of irisin to induce the browning of inguinal fat in HFD-fed mice.

To identify the changes in gene expression in the process of browning of WAT, the differentially expressed genes (DEGs) were assessed with a microarray data mining strategy. As shown in Figure 8a, the top 50 up-regulated genes ranked by log2 fold changes were used to generate a heatmap. These genes were used as input list to search against the STRING database. The network was shown in Figure 8b. Briefly, 39 nodes were mapped against the STRING database, and 25 edges were generated. The average node degree is 1.28. Moreover, the *P* value of protein–protein interaction enrichment is lower than 1e − 16. PPAR signalling pathway (KO03320, FDR = 6.32e − 05) and adipokine signalling pathway (KO04920, FDR = 0.0276) were significantly enriched. The most striking finding of microarray data mining was the marked up-regulation of beige adipocyte markers in the subcluster shown in Figure 8c, including cell death-inducing DNA fragmentation factor α-like effector A (*Cidea*), *Ucp1*, *Ppara*, *Cd36*, and *Cox7a1*. Furthermore, real-time PCR results showed that HFD feeding reduced the expression levels of *Ucp1*, *Cox7a*, *Cidea*, and *Ppara* in inguinal fat, whereas myricanol administration reversed these changes (Figure 8d).

4 | DISCUSSION

Skeletal muscle is the most important tissue involved in insulin-stimulated glucose disposal, and insulin resistance in skeletal muscle is a major defect in most obese phenotypes (Leonard, Watson, Loomes, Phillips, & Cooper, 2005). Serum free fatty acids are an important fuel source for skeletal muscle. Accumulation of excessive lipid metabolites in skeletal muscle contributes to insulin resistance (Koves et al., 2008). In most obese phenotypes, the accumulation of lipid exceeds the oxidation capacity, and incomplete lipid metabolic products, such as acyl-CoA, DAG and ceramide, are generated (Abdul-Ghani et al., 2008). These products inhibit the activation of critical molecules involved in insulin signalling, such as AKT and IRS, leading to insulin resistance in skeletal muscle (Itani, Zhou, Pories, MacDonald, & Dohm, 2000). Treatments enhancing lipid consumption and mobilizing lipid out of skeletal muscle lead to enhanced insulin sensitivity (Schrauwen, Schrauwen-Hinderling, Hoeks, & Hesselink, 2010). In our experiments, myricanol was found to reduce lipid accumulation in PA-treated C2C12 myotubes and skeletal muscle from HFD-fed mice, which in turn enhanced insulin sensitivity.

Activation of AMPK induces catabolic pathways and the generation of ATP under nutrient deprivation (Hardie, 2007). AMPK regulates fatty acid metabolism and mitochondrial biogenesis in response to pharmacological activation as well as exercise, which makes AMPK a potential therapeutic target for treatment of obesity and Type 2 diabetes. Previous studies from diabetic rodents and human subjects demonstrated that pharmacological agents, such as AICAR (Koistinen et al., 2003) and **metformin** (Wu et al., 2015), increase glucose uptake and enhance insulin sensitivity in skeletal muscle via activating AMPK. Our previous study found that myricanol directly binds to the γ subunit of AMPK and activates AMPK, to suppress adipogenesis and induce lipolysis and lipid combustion in adipocytes (Shen, Liao, Feng, et al., 2019). The present study further confirmed that myricanol activated AMPK in PA-treated C2C12 myotubes and skeletal muscle from HFD-fed mice, to reduce lipid accumulation and enhance insulin sensitivity.

PA is widely used to induce mitochondrial dysfunction and insulin resistance in C2C12 myotubes. The PA-treated cells exhibit reduced

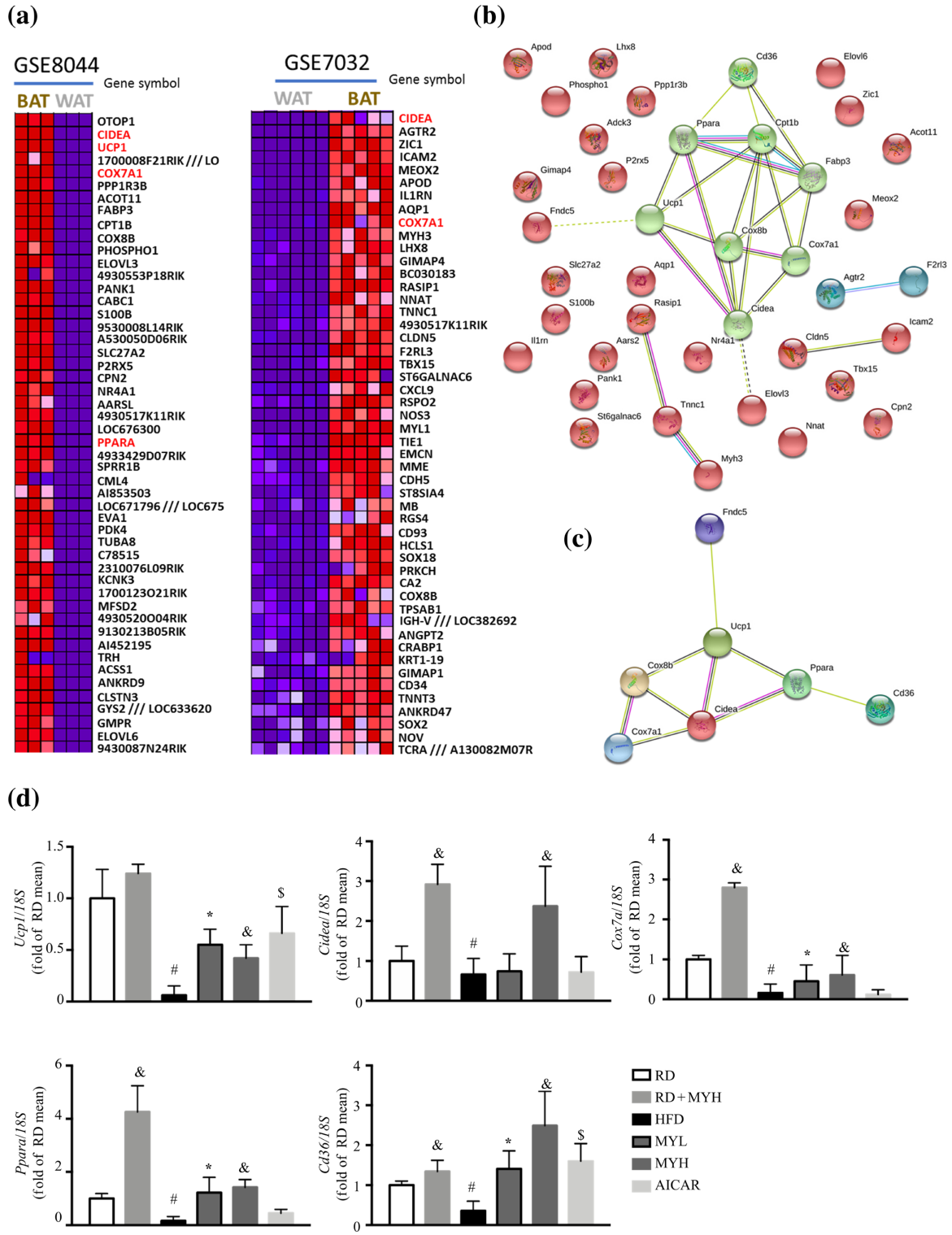

FIGURE 8 Data mining using microarray data from GEO database. Two microarray datasets were retrieved from GEO database to mine the significant differential expressed genes between brown adipose tissue (BAT) and white adipose tissue (WAT) from mice. (a) Heatmap of the top 50 differentially expressed genes in the two datasets after analysis using GEO2R and GSEA. (b) Protein–protein interaction map of the differentially expressed genes generated using STRING. (c) Interaction map of the enriched significant pathways clustered by *K*-means. (d) Real-time RT-PCR analyses of *Ucp1*, *Cidea*, *Cox7a*, and *Ppara* in inguinal WAT ($n = 6$). Data are shown as mean ± SD. $^{*}P < .05$, low dose myricanol (MYL) significantly different from high-fat diet (HFD). $^{\&}P < .05$, high dose myricanol (MYH) significantly different from HFD or regular chow diet (RD) significantly different from RD + MYH. $^{\#}P < .05$, RD significantly different from HFD. $^{\$}P < .05$, AICAR significantly different from HFD. Differences between two treatment groups were assessed using one-way ANOVA followed by independent-samples' t-test. For multiple comparisons, one-way or two-way ANOVA with Bonferroni's correction was applied

levels of ATP production and mitochondrial DNA, accompanied with reduced mitochondrial oxygen consumption. PA activates AMPK at concentrations lower than 100 μmol·L^{-1} and suppresses the phosphorylation of AMPK at the concentration higher than 200 μmol·L^{-1} (Fediuc, Gaidhu, & Ceddia, 2006). Here, 250 μmol·L^{-1} of PA was used to induce lipid accumulation and insulin resistance in C2C12 myotubes.

Mitochondrial dysfunction in skeletal muscle has been suggested to underlie the development of insulin resistance and Type 2 diabetes. It should be noted that lipid-induced mitochondrial dysfunction, termed lipotoxicity, leads to progressive deterioration of muscular oxidative capacity and the accumulation of lipid intermediates in skeletal muscle (Schrauwen et al., 2010). Mitochondrial function is determined not only by intrinsic mitochondrial function but also by mitochondrial content and even substrate supply to the skeletal muscle. Mitochondrial biogenesis is regulated by the family of PGC-1 transcription cofactors, including PGC-1α and PGC-1β (Romanello & Sandri, 2013). PGC-1α directly interacts with the nuclear respiratory factor 1 and modulates its target, mitochondrial transcription factor A, to translocate to the mitochondria and activate mitochondrial DNA replication, resulting in increased mitochondrial biogenesis (Wu et al., 1999). Currently, myricanol increases PGC-1α expression, to reverse PA-induced mitochondrial dysfunction and enhance muscle function in HFD-fed mice. These results provide evidence that myricanol treatment could stimulate mitochondrial biogenesis, increase mitochondrial oxidative metabolism, and benefit ATP synthesis.

There is accumulating evidence that the morphological transition from WAT to BAT, a process termed "browning", facilitates the treatment of obesity. The browning of WAT is always associated with an increase of mitochondria content and enhancement of energy metabolism with increased oxygen consumption, which means switching from an energy storage state to an energy dissipation state and expressing specific molecular markers, such as UCP1 (Kajimura, Seale, & Spiegelman, 2010; Liu & Lin, 2019). UCP1 constitutes the most specific difference in the biochemical characteristics of white and brown adipocytes, which is only expressed in the mitochondria in brown adipocytes and beige cells (Dempersmier et al., 2015). Recent studies have identified several dominant transcriptional regulators of brown adipocyte development and function, including PPARγ, PGC-1α, and PR domain containing 16 (PRDM16; Seale, 2015). PPARγ is expressed abundantly and at equal levels in white and brown fat and is required for the development of both cell types. PPARγ is recognized as a master regulator of adipogenesis, and its activation or inhibition is not adequate or sufficient for white-to-brown adipocyte transition (Farmer, 2006). In addition, PGC-1α is of particular importance, given its roles in up-regulating UCP1 expression and the uncoupling of mitochondrial fat combustion for ATP production (Becerril et al., 2013). The induction of browning is highly adipose depot dependent. In mice, the subcutaneous WAT undergoes the most profound induction of browning, whereas the epididymal WAT is particularly resistant to "browning," and the interscapular WAT contains bipotent adipogenic precursor cells that can give rise to both white and beige adipocytes, depending on environmental conditions (Lee, Petkova, Mottillo, & Granneman, 2012). The inguinal WAT is a major subcutaneous depot that expresses relatively high levels of PRDM16 and has an inherently high browning response (Seale et al., 2011).

Irisin was discovered as a key exercise-induced myokine that promotes browning of WAT and increases energy expenditure (Boström et al., 2012; Huh et al., 2012). Irisin induces UCP1 expression and increases energy expenditure in human adipocytes, resulting in reduced lipid accumulation (Huh et al., 2014). Treatment with irisin increases mitochondrial oxidative metabolism, mitochondrial uncoupling, and fatty acid oxidation in skeletal muscle (Xin et al., 2016). Myricanol induces irisin production and secretion in both C2C12 myocytes and skeletal muscle from HFD-fed mice through the AMPK/PGC-1α pathway. Irisin plays a key role in the crosstalk between adipose tissue and skeletal muscle, mediating the effect of myricanol in enhancing the fat browning. Besides irisin, several cytokine and myokines have identified as the positive regulators, such as **IL-6**, β-aminoisobutyric acid, and meteorin-like protein (METRNL), or the negative regulator, such as myostatin, of fat browning (Knudsen et al., 2014; Roberts et al., 2014; Rodriguez, Becerril, Ezquerro, Mendez-Gimenez, & Fruhbeck, 2017; Shan, Liang, Bi, & Kuang, 2013). Lactate, a metabolite released by skeletal muscle during and after exercise, also induces a robust increase of the thermogenic gene expression in mouse and human white adipocytes through PPARγ activation (Carriere et al., 2014). Thus, myricanol might regulate the release of myokines and/or lactate to induce the browning of adipose tissue.

Notably, irisin directly promotes skeletal muscle accretion by increasing myogenesis and decreasing myostatin and atrophy-related genes (Huh et al., 2014; Rodriguez, Ezquerro, Mendez-Gimenez, Becerril, & Fruhbeck, 2015). Moreover, the adipose tissue also expresses the *Fndc5* gene and secrets irisin, as well as constituting a target of irisin (Moreno-Navarrete et al., 2013). This evidence indicated that irisin is not only a myokine but also an adipokine. Exercise induces PGC-1α expression, which in turn activates the expression and secretion of irisin, β-aminoisobutyric acid, and METRNL in myocytes. However, it needs to be elucidated whether the adipose tissue secretes feedback signals to close the myocyte–adipocyte circle. **Leptin** regulates irisin-induced browning process in autocrine/paracrine manner (Rodriguez, Ezquerro, et al., 2015). The dysregulation of adipokines

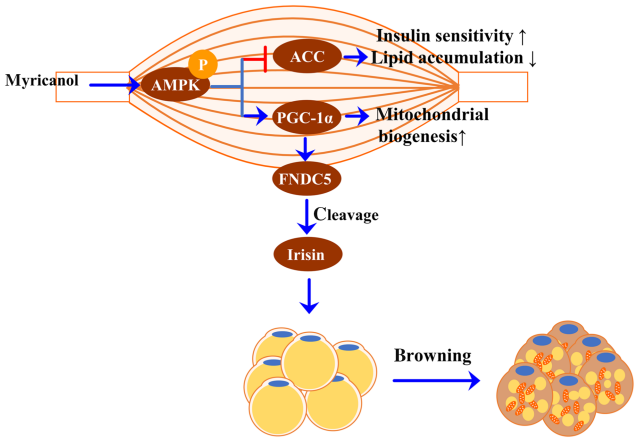

FIGURE 9 Diagram of molecular targets of myricanol in modulating crosstalk between adipose tissue and skeletal muscle

and myokines might favour the development of excess adiposity (Rodriguez et al., 2017). Although the current data could not exclude a direct effect of myricanol on adipocytes, it provides crucial insights into the role of adipose tissue–skeletal muscle communication in treating insulin resistance and obesity.

In summary, myricanol was found to alleviate lipid accumulation in PA-treated myotubes in vitro and skeletal muscle from HFD-fed mice in vivo. Myricanol enhanced insulin sensitivity *via* promoting mitochondrial biogenesis and function. Moreover, myricanol induced irisin production in PA-treated myotubes and HFD-fed mice through the AMPK/PGC-1α signalling pathway, to induce WAT browning (Figure 9). Taken together, myricanol provides insightful perspectives on the communication between adipose tissue and skeletal muscle, and this compound could be developed as a candidate for treatment of insulin resistance and obesity.

ACKNOWLEDGEMENTS

Financial support by the National Natural Science Foundation of China (81872754), The Science and Technology Development Fund, Macau SAR (File no. FDCT 0031/2019/A1), and the Research Fund of Universidade de Macau (MYRG2017-00109-ICMS and MYRG2018-00037-ICMS) are gratefully acknowledged.

AUTHOR CONTRIBUTIONS

S.S., Q.L., and T.Z. conducted the research and analysed the data; S.S. and L.L. designed the experiments and wrote the paper; R.P. consulted for the study and proofread the paper; and L.L. conceived the study.

CONFLICT OF INTEREST

The authors declare no conflicts of interest.

DECLARATION OF TRANSPARENCY AND SCIENTIFIC RIGOUR

This Declaration acknowledges that this paper adheres to the principles for transparent reporting and scientific rigour of preclinical research as stated in the *BJP* guidelines for Design & Analysis, Immunoblotting and Immunochemistry, and Animal Experimentation and as recommended by funding agencies, publishers, and other organizations engaged with supporting research.

ORCID

Ligen Lin https://orcid.org/0000-0002-6799-5327

REFERENCES

Abdul-Ghani, M. A., Muller, F. L., Liu, Y., Chavez, A. O., Balas, B., Zuo, P., … Molina-Carrion, M. (2008). Deleterious action of FA metabolites on ATP synthesis: Possible link between lipotoxicity, mitochondrial dysfunction, and insulin resistance. *American Journal of Physiology-Endocrinology and Metabolism*, *295*, E678–E685. https://doi.org/10.1152/ajpendo.90287.2008

Alexander, S. P. H., Cidlowski, J. A., Kelly, E., Marrion, N. V., Peters, J. A., Faccenda, E., … Collaborators, C. G. T. P. (2017). The Concise Guide to PHARMACOLOGY 2017/18: Nuclear hormone receptors. *British Journal of Pharmacology*, *174*, S208–S224. https://doi.org/10.1111/bph.13880

Alexander, S. P., Fabbro, D., Kelly, E., Marrion, N. V., Peters, J. A., Faccenda, E., … CGTP Collaborators (2017). The Concise Guide to PHARMACOLOGY 2017/18: Enzymes. *British Journal of Pharmacology*, *174*(Suppl 1), S272–S359. https://doi.org/10.1111/bph.13877

Alexander, S. P. H., Kelly, E., Marrion, N. V., Peters, J. A., Faccenda, E., Harding, S. D., … Collaborators, C. G. T. P. (2017). The Concise Guide to PHARMACOLOGY 2017/18: Transporters. *British Journal of Pharmacology*, *174*, S360–S446. https://doi.org/10.1111/bph.13883

Alexander, S. P. H., Roberts, R. E., Broughton, B. R., Sobey, C. G., George, C. H., Stanford, S. C., … Ahluwalia, A. (2018). Goals and practicalities of immunoblotting and immunohistochemistry: A guide for submission to the *British Journal of Pharmacology*. *British Journal of Pharmacology*, *175*, 407–411. http://doi.org/10.1111/bph.14112

Altshuler-Keylin, S., & Kajimura, S. (2017). Mitochondrial homeostasis in adipose tissue remodeling. *Science Signaling*, *10*, pii: eaai9248. https://doi.org/10.1126/scisignal.aai9248

Becerril, S., Gomez-Ambrosi, J., Martin, M., Moncada, R., Sesma, P., Burrell, M. A., & Fruhbeck, G. (2013). Role of PRDM16 in the activation of brown fat programming. Relevance to the development of obesity. *Histology and Histopathology*, *28*, 1411–1425. https://doi.org/10.14670/HH-28.1411

Benjamini, Y., & Yekutieli, D. (2001). The control of the false discovery rate in multiple testing under dependency. *Annals of Statistics*, *29*, 1165–1188. https://doi.org/10.1214/aos/1013699998

Bonora, E., Zavaroni, I., Alpi, O., Pezzarossa, A., Dall'Aglio, E., Coscelli, C., & Butturini, U. (1987). Influence of the menstrual cycle on glucose tolerance and insulin secretion. *American Journal of Obstetrics and Gynecology*, *157*, 140–141. https://doi.org/10.1016/s0002-9378(87)80365-4

Boström, P., Wu, J., Jedrychowski, M. P., Korde, A., Ye, L., Lo, J. C., … Long, J. Z. (2012). A PGC1-α-dependent myokine that drives brown-fat-like development of white fat and thermogenesis. *Nature*, *481*, 463–468. https://doi.org/10.1038/nature10777

Carriere, A., Jeanson, Y., Berger-Muller, S., Andre, M., Chenouard, V., Arnaud, E., … Casteilla, L. (2014). Browning of white adipose cells by intermediate metabolites: An adaptive mechanism to alleviate redox pressure. *Diabetes*, *63*, 3253–3265. https://doi.org/10.2337/db13-1885

Chaudhury, A., Duvoor, C., Dendi, V. S. R., Kraleti, S., Chada, A., Ravilla, R., … Mirza, W. (2017). Clinical review of antidiabetic drugs: Implications for type 2 diabetes mellitus management. *Frontiers in Endocrinology*, *8*, 6. https://doi.org/10.3389/fendo.2017.00006

Curtis, M. J., Alexander, S., Cirino, G., Docherty, J. R., George, C. H., Giembycz, M. A., … Ahluwalia, A. (2018). Experimental design and analysis and their reporting II: Updated and simplified guidance for authors and peer reviewers. *British Journal of Pharmacology*, *175*, 987–993. https://doi.org/10.1111/bph.14153

Davis, S., & Meltzer, P. S. (2007). GEOquery: A bridge between the Gene Expression Omnibus (GEO) and BioConductor. *Bioinformatics*, *23*, 1846–1847. https://doi.org/10.1093/bioinformatics/btm254

DeFronzo, R. A., & Tripathy, D. (2009). Skeletal muscle insulin resistance is the primary defect in type 2 diabetes. *Diabetes Care*, *32*, S157–S163. https://doi.org/10.2337/dc09-S302

Demirpence, M., Yilmaz, H., Colak, A., Yalcin, H., Toprak, B., Turkon, H., … Aydin, C. (2016). The effect of sleeve gastrectomy on serum irisin levels in patients with morbid obesity. *Endokrynologia Polska*, *67*, 481–486. https://doi.org/10.5603/EP.a2016.0029

Dempersmier, J., Sambeat, A., Gulyaeva, O., Paul, S. M., Hudak, C. S., Raposo, H. F., … Sul, H. S. (2015). Cold-inducible Zfp516 activates

UCP1 transcription to promote browning of white fat and development of brown fat. *Molecular Cell*, *57*, 235–246. https://doi.org/10.1016/j.molcel.2014.12.005

Farmer, S. R. (2006). Transcriptional control of adipocyte formation. *Cell Metabolism*, *4*, 263–273. https://doi.org/10.1016/j.cmet.2006.07.001

Fediuc, S., Gaidhu, M. P., & Ceddia, R. B. (2006). Regulation of AMP-activated protein kinase and acetyl-CoA carboxylase phosphorylation by palmitate in skeletal muscle cells. *Journal of Lipid Research*, *47*, 412–420. https://doi.org/10.1194/jlr.M500438-JLR200

Fedorenko, A., Lishko, P. V., & Kirichok, Y. (2012). Mechanism of fatty-acid-dependent UCP1 uncoupling in brown fat mitochondria. *Cell*, *151*, 400–413. https://doi.org/10.1016/j.cell.2012.09.010

Feng, Z. L., Zhang, L. L., Zheng, Y. D., Liu, Q. Y., Liu, J. X., Feng, L., … Lin, L. G. (2017). Norditerpenoids and dinorditerpenoids from the seeds of *Podocarpus nagi* as cytotoxic agents and autophagy inducers. *Journal of Natural Products*, *80*, 2110–2117. https://doi.org/10.1021/acs.jnatprod.7b00347

Hardie, D. G. (2007). AMP-activated/SNF1 protein kinases: Conserved guardians of cellular energy. *Nature Review Molecular Cell Biology*, *8*, 774–785. https://doi.org/10.1038/nrm2249

Harding, S. D., Sharman, J. L., Faccenda, E., Southan, C., Pawson, A. J., Ireland, S., … NC-IUPHAR (2018). The IUPHAR/BPS Guide to PHARMACOLOGY in 2018: Updates and expansion to encompass the new guide to IMMUNOPHARMACOLOGY. *Nucleic Acids Research*, *46*, D1091–D1106. http://doi.org/10.1093/nar/gkx1121

Huh, J. Y., Mougios, V., Kabasakalis, A., Fatouros, I., Siopi, A., Douroudos, I. I., … Mantzoros, C. S. (2014). Exercise-induced irisin secretion is independent of age or fitness level and increased irisin may directly modulate muscle metabolism through AMPK activation. *Journal of Clinical Endocrinology & Metabolism*, *99*, E2154–E2161. https://doi.org/10.1210/jc.2014-1437

Huh, J. Y., Panagiotou, G., Mougios, V., Brinkoetter, M., Vamvini, M. T., Schneider, B. E., & Mantzoros, C. S. (2012). FNDC5 and irisin in humans: I. Predictors of circulating concentrations in serum and plasma and II. mRNA expression and circulating concentrations in response to weight loss and exercise. *Metabolism*, *61*, 1725–1738. https://doi.org/10.1016/j.metabol.2012.09.002

de la Iglesia, R., Lopez-Legarrea, P., Crujeiras, A. B., Pardo, M., Casanueva, F. F., Zulet, M. A., & Martinez, J. A. (2014). Plasma irisin depletion under energy restriction is associated with improvements in lipid profile in metabolic syndrome patients. *Clinical Endocrinology*, *81*, 306–311. https://doi.org/10.1111/cen.12383

International Diabetes Federation (2017). *IDF diabetes atlas* (8th ed.). Brussels, Belguim: International Diabetes Federation.

Itani, S. I., Zhou, Q., Pories, W. J., MacDonald, K. G., & Dohm, G. L. (2000). Involvement of protein kinase C in human skeletal muscle insulin resistance and obesity. *Diabetes*, *49*, 1353–1358. https://doi.org/10.2337/diabetes.49.8.1353

Kahn, B. B., Alquier, T., Carling, D., & Hardie, D. G. (2005). AMP-activated protein kinase: Ancient energy gauge provides clues to modern understanding of metabolism. *Cell Metabolism*, *1*, 15–25. https://doi.org/10.1016/j.cmet.2004.12.003

Kajimura, S., Seale, P., & Spiegelman, B. M. (2010). Transcriptional control of brown fat development. *Cell Metabolism*, *11*, 257–262. https://doi.org/10.1016/j.cmet.2010.03.005

Kilkenny, C., Browne, W., Cuthill, I. C., Emerson, M., & Altman, D. G. (2010). Animal research: Reporting in vivo experiments: The ARRIVE guidelines. *British Journal of Pharmacology*, *160*, 1577–1579. https://doi.org/10.1111/j.1476-5381.2010.00872.x

Knudsen, J. G., Murholm, M., Carey, A. L., Bienso, R. S., Basse, A. L., Allen, T. L., … Pilegaard, H. (2014). Role of IL-6 in exercise training- and cold-induced UCP1 expression in subcutaneous white adipose tissue. *PLoS ONE*, *9*, e84910. https://doi.org/10.1371/journal.pone.0084910

Koistinen, H. A., Galuska, D., Chibalin, A. V., Yang, J., Zierath, J. R., Holman, G. D., & Wallberg-Henriksson, H. (2003). 5-amino-imidazole carboxamide riboside increases glucose transport and cell-surface GLUT4 content in skeletal muscle from subjects with type 2 diabetes. *Diabetes*, *52*, 1066–1072. https://doi.org/10.2337/diabetes.52.5.1066

Koves, T. R., Ussher, J. R., Noland, R. C., Slentz, D., Mosedale, M., Ilkayeva, O., … Muoio, D. M. (2008). Mitochondrial overload and incomplete fatty acid oxidation contribute to skeletal muscle insulin resistance. *Cell Metabolism*, *7*, 45–56. https://doi.org/10.1016/j.cmet.2007.10.013

Kraegen, E. W., & Cooney, G. J. (2008). Free fatty acids and skeletal muscle insulin resistance. *Current Opinion in Lipidology*, *19*, 235–241. https://doi.org/10.1097/01.mol.0000319118.44995.9a

Kurdiova, T., Balaz, M., Mayer, A., Maderova, D., Belan, V., Wolfrum, C., … Ukropcova, B. (2014). Exercise-mimicking treatment fails to increase Fndc5 mRNA & irisin secretion in primary human myotubes. *Peptides*, *56*, 1–7. https://doi.org/10.1016/j.peptides.2014.03.003

Lee, Y. H., Petkova, A. P., Mottillo, E. P., & Granneman, J. G. (2012). *In vivo* identification of bipotential adipocyte progenitors recruited by β3-adrenoceptor activation and high-fat feeding. *Cell Metabolism*, *15*, 480–491. https://doi.org/10.1016/j.cmet.2012.03.009

Leonard, B. L., Watson, R. N., Loomes, K. M., Phillips, A. R. J., & Cooper, G. J. (2005). Insulin resistance in the Zucker diabetic fatty rat: A metabolic characterisation of obese and lean phenotypes. *Acta Diabetologica*, *42*, 162–170. https://doi.org/10.1007/s00592-005-0197-8

Li, D., Liu, Q. Y., Sun, W., Chen, X. P., Wang, Y., Sun, Y. X., & Lin, L. G. (2018). 1,3,6,7-Tetrahydroxy-8-prenylxanthone ameliorates inflammatory responses resulting from the paracrine interaction of adipocytes and macrophages. *British Journal of Pharmacology*, *175*, 1590–1606. https://doi.org/10.1111/bph.14162

Lin, L. G., Lee, J. H., Bongmba, O. Y., Ma, X. J., Zhu, X. W., Sheikh-Hamad, D., & Sun, Y. X. (2014). The suppression of ghrelin signaling mitigates age-associated thermogenic impairment. *Aging*, *6*, 1019–1032. https://doi.org/10.18632/aging.100706

Lin, L. G., Pang, W. J., Chen, K. Y., Wang, F., Gengler, J., Sun, Y. X., & Tong, Q. (2012). Adipocyte expression of PU.1 transcription factor causes insulin resistance through upregulation of inflammatory cytokine gene expression and ROS production. *American Journal of Physiology-Endocrinology and Metabolism*, *302*, E1550–E1559. https://doi.org/10.1152/ajpendo.00462.2011

Liu, J. X., & Lin, L. G. (2019). Small molecules for fat combustion: Targeting thermosensory and satiety signals in the central nervous system. *Drug Discovery Today*, *24*, 300–306. https://doi.org/10.1016/j.drugdis.2018.09.013

Moreno-Navarrete, J. M., Ortega, F., Serrano, M., Guerra, E., Pardo, G., Tinahones, F., … Fernandez-Real, J. M. (2013). Irisin is expressed and produced by human muscle and adipose tissue in association with obesity and insulin resistance. *Journal of Clinical Endocrinology and Metabolism*, *98*, E769–E778. https://doi.org/10.1210/jc.2012-2749

Pardo, M., Crujeiras, A. B., Amil, M., Aguera, Z., Jimenez-Murcia, S., Banos, R., … Casanueva, F. F. (2014). Association of irisin with fat mass, resting energy expenditure, and daily activity in conditions of extreme body mass index. *International Journal of Endocrinology*, *2014*, 857270–857279. https://doi.org/10.1155/2014/857270

Roberts, L. D., Bostrom, P., O'Sullivan, J. F., Schinzel, R. T., Lewis, G. D., Dejam, A., … Gerszten, R. E. (2014). β-Aminoisobutyric acid induces browning of white fat and hepatic β-oxidation and is inversely correlated with cardiometabolic risk factors. *Cell Metabolism*, *19*, 96–108. https://doi.org/10.1016/j.cmet.2013.12.003

Rodriguez, A., Becerril, S., Ezquerro, S., Mendez-Gimenez, L., & Fruhbeck, G. (2017). Crosstalk between adipokines and myokines in fat browning. *Acta Physiology*, *219*, 362–381. https://doi.org/10.1111/apha.12686

Rodriguez, A., Becerril, S., Mendez-Gimenez, L., Ramirez, B., Sainz, N., Catalan, V., … Fruhbeck, G. (2015). Leptin administration activates irisin-induced myogenesis via nitric oxide-dependent mechanisms, but reduces its effect on subcutaneous fat browning in mice. *International Journal of Obesity*, *39*, 397–407. https://doi.org/10.1038/ijo.2014.166

Rodriguez, A., Ezquerro, S., Mendez-Gimenez, L., Becerril, S., & Fruhbeck, G. (2015). Revisiting the adipocyte: A model for integration of cytokine signaling in the regulation of energy metabolism. *American Journal of Physiology-Endocrinology and Metabolism*, *309*, E691–E714. https://doi.org/10.1152/ajpendo.00297.2015

Romanello, V., & Sandri, M. (2013). Mitochondrial biogenesis and fragmentation as regulators of protein degradation in striated muscles. *Journal of Molecular and Cellular Cardiology*, *55*, 64–72. https://doi.org/10.1016/j.yjmcc.2012.08.001

Schrauwen, P., Schrauwen-Hinderling, V., Hoeks, J., & Hesselink, M. K. C. (2010). Mitochondrial dysfunction and lipotoxicity. *Biochimica et Biophysica Acta-Molecular and Cell Biology of Lipids*, *1801*, 266–271. https://doi.org/10.1016/j.bbalip.2009.09.011

Seale, P. (2015). Transcriptional regulatory circuits controlling brown fat development and activation. *Diabetes*, *64*, 2369–2375. https://doi.org/10.2337/db15-0203

Seale, P., Conroe, H. M., Estall, J., Kajimura, S., Frontini, A., Ishibashi, J., … Spiegelman, B. M. (2011). Prdm16 determines the thermogenic program of subcutaneous white adipose tissue in mice. *Journal of Clinical Investigation*, *121*, 96–105. https://doi.org/10.1172/JCI44271

Seale, P., Kajimura, S., Yang, W., Chin, S., Rohas, L. M., Uldry, M., … Spiegelman, B. M. (2007). Transcriptional control of brown fat determination by PRDM16. *Cell Metabolism*, *6*, 38–54. https://doi.org/10.1016/j.cmet.2007.06.001

Shan, T., Liang, X., Bi, P., & Kuang, S. (2013). Myostatin knockout drives browning of white adipose tissue through activating the AMPK–PGC1α–Fndc5 pathway in muscle. *FASEB Journal*, *27*, 1981–1989. https://doi.org/10.1096/fj.12-225755

Shen, S. N., Liao, Q. W., Feng, Y., Liu, J. X., Pan, R. L., Lee, S. M., & Lin, L. G. (2019). Myricanol mitigates lipid accumulation in 3T3-L1 adipocytes and high fat diet-fed zebrafish via activating AMP-activated protein kinase. *Food Chemistry*, *270*, 305–314. https://doi.org/10.1016/j.foodchem.2018.07.117

Shen, S. N., Liao, Q. W., Huang, L., Li, D., Zhang, Q. W., Wang, Y. T., … Lin, L. G. (2018). Water soluble fraction from ethanolic extract of *Clausena lansium* seeds alleviates obesity and insulin resistance, and changes the composition of gut microbiota in high-fat diet-fed mice. *Journal of Functional Foods*, *47*, 192–199. https://doi.org/10.1016/j.jff.2018.05.057

Shen, S. N., Liao, Q. W., Liu, J. X., Pan, R. L., Lee, S. M., & Lin, L. G. (2019). Myricanol rescues dexamethasone-induced muscle dysfunction via a sirtuin 1-dependent mechanism. *Journal of Cachexia Sarcopenia Muscle*, *10*, 429–444. http://doi.org/10.1002/jcsm.12393

Stengel, A., Hofmann, T., Goebel-Stengel, M., Elbelt, U., Kobelt, P., & Klapp, B. F. (2013). Circulating levels of irisin in patients with anorexia nervosa and different stages of obesity—Correlation with body mass index. *Peptides*, *39*, 125–130. https://doi.org/10.1016/j.peptides.2012.11.014

Szklarczyk, D., Franceschini, A., Wyder, S., Forslund, K., Heller, D., Huerta-Cepas, J., … von Mering, C. (2015). STRING v10: Protein–protein interaction networks, integrated over the tree of life. *Nucleic Acids Research*, *43*, D447–D452. https://doi.org/10.1093/nar/gku1003

Timmons, J. A., Wennmalm, K., Larsson, O., Walden, T. B., Lassmann, T., Petrovic, N., … Cannon, B. (2007). Myogenic gene expression signature establishes that brown and white adipocytes originate from distinct cell lineages. *Proceedings of the National Academy of Sciences of the United States*, *104*, 4401–4406. https://doi.org/10.1073/pnas.0610615104

Wu, W. J., Tang, S. Y. Y., Shi, J. F., Yin, W. W., Cao, S., Bu, R. F., … Bi, Y. (2015). Metformin attenuates palmitic acid-induced insulin resistance in L6 cells through the AMP-activated protein kinase/sterol regulatory element-binding protein-1c pathway. *International Journal of Molecular Medicine*, *35*, 1734–1740. https://doi.org/10.3892/ijmm.2015.2187

Wu, Z. D., Puigserver, P., Andersson, U., Zhang, C. Y., Adelmant, G., Mootha, V., … Spiegelman, B. M. (1999). Mechanisms controlling mitochondrial biogenesis and respiration through the thermogenic coactivator PGC-1. *Cell*, *98*, 115–124. https://doi.org/10.1016/S0092-8674(00)80611-X

Xin, C., Liu, J., Zhang, J., Zhu, D., Wang, H., Xiong, L., … Tao, L. (2016). Irisin improves fatty acid oxidation and glucose utilization in type 2 diabetes by regulating the AMPK signaling pathway. *International Journal of Obesity*, *40*, 443–451. https://doi.org/10.1038/ijo.2015.199

SUPPORTING INFORMATION

Additional supporting information may be found online in the Supporting Information section at the end of the article.

How to cite this article: Shen S, Liao Q, Zhang T, Pan R, Lin L. Myricanol modulates skeletal muscle–adipose tissue crosstalk to alleviate high-fat diet-induced obesity and insulin resistance. *Br J Pharmacol*. 2019;176:3983–4001. https://doi.org/10.1111/bph.14802